THE UNIVERSITY OF MICHIGAN

COLLEGE OF ENGINEERING
Department of Aeronautical and Astronautical Engineering
Aircraft Propulsion Laboratory

Quarterly Progress Report No. 2
(1 September 1962 to 30 November 1962)

THE FEASIBILITY OF A ROTATING DETONATION WAVE ROCKET MOTOR

J. A. Nicholls
R. E. Cullen
T. C. Adamson
G. L. Cosens
M. Sichel
E. Kurath
F. Cheslak
G. Olsson
J. Fu
T. David
J. Brown
K. Ragland
S. Schmidt

ORA Project 05179

under contract with:

AIR FORCE FLIGHT TEST CENTER
6593d TEST GROUP (DEVELOPMENT)
CONTRACT NO. AF 04(611)-8503
EDWARDS AIR FORCE BASE, CALIFORNIA

administered through:

OFFICE OF RESEARCH ADMINISTRATION ANN ARBOR

December 1962

TABLE OF CONTENTS

LIST OF TABLES

LIST OF FIGURES

NOMENCLATURE

PART I-A

We	Weber number
$(We)_{cr}$	critical Weber number
U	relative velocity between the gas and the droplets
S	surface tension
ρ_g	density of the gas
r	radius of the droplet
ρ_ℓ	density of the liquid
D	diameter of the droplet
μ_ℓ	viscosity of the liquid
Re	Reynolds number
L_B	distance traversed by the detonation wave front during droplet breakup time
L_C	distance between the initial shock wave front and the zone of significant chemical reaction
t_b	droplet breakup time

PART I-B

Le	Lewis number = $\overline{C}_p D\rho/k$
D	binary diffusion coefficient
ρ	density
k	thermal conductivity
X_i	mole-fraction of species i

PART I-B (Concluded)

h	enthalpy per unit mass
τ	shear stress at the wall
Pr	Prandtl number = $(C_p\mu)/k$
μ	viscosity
V_D	detonation velocity
W_i	molecular weight of species i
$\overline{W}$	average molecular weight of a mixture
q_w	heat flux per unit area at the wall
x	distance from the detonation wave
$\overline{Q}_w$	overall average heat flux per unit area to walls of chamber
V	velocity
h_r	adiabatic recovery enthalpy
T_c	temperature in conventional combustion chamber
T	temperature

Subscripts

e	free stream conditions behind detonation
m	reference conditions

PART I-C

a (ft/sec)	local speed of sound
A (ft^2)	area
A_c (ft^2)	chamber cross sectional area, $\ell_c x_n$

PART I-C (Continued)

A_s	(ft^2)	convergent nozzle sectional area
B	-	area ratio parameter, $(\frac{2}{\gamma+1})^{\frac{\gamma+1}{2(\gamma-1)}} \frac{\ell_t L}{A_c}$
b,c	-	constants introduced in the solution of the jump conditions
C_p	$(\frac{ft\text{-}lb}{slug\text{-}^\circ R})$	specific heat at constant pressure
D	-	determinant of the coefficients
G	-	mass flow parameter, $\dot{m}_p/\rho_o v_o A_c N$
h	$(\frac{ft\text{-}lb}{slug})$	specific enthalpy
$h^{(o)}$	$(\frac{ft\text{-}lb}{slug})$	specific enthalpy at absolute zero
h_p	$(\frac{ft\text{-}lb}{slug})$	initial propellant specific enthalpy
ℓ_c	(ft)	radial width of the chamber
ℓ_t	(ft)	width of the nozzle throat
L	(ft)	distance between detonation waves, $2\pi R/N$
$\dot{m}$	$(\frac{slugs}{sec})$	mass flow rate
$\dot{m}_p$	$(\frac{slugs}{sec})$	total propellant mass flow rate
$\bar{m}$	$mole^{-1}$	average molecular weight
M	-	Mach number
n	(ft)	coordinate normal to streamlines in the radial direction
N	-	number of waves in the engine
P	(lb/ft^2)	absolute pressure

PART I-C (Continued)

Q	$(\frac{\text{ft-lb}}{\text{slug}})$	heat added per unit mass of unburned propellant
$\overline{Q}$	-	heat addition parameter, Q/C_pT_o
R	(ft)	radius of curvature of the chamber centerline
R_o	$(\frac{\text{ft-lb}}{\text{slug mol-°R}})$	universal gas constant
T	(°R)	absolute temperature
t	(sec)	time
u,v	(ft/sec)	axial and circumferential velocity components
V	(ft/sec)	magnitude of the velocity
V_w	(ft/sec)	absolute detonation wave velocity
x,y	(ft)	axial and circumferential coordinates
γ	-	ratio of specific heats
η	-	dimensionless circumferential coordinate, y/L
ξ	-	dimensionless axial coordinate, x/x_n
μ	-	relative mass concentration of the unburned propellant
ρ	$(\frac{\text{slugs}}{\text{ft}^3})$	mass density

Subscripts

0	refers to condition at $y = 0$
1	refers to condition at $y = L$
a	refers to absolute velocity
A	refers to the unburned propellant
B	refers to the burned propellant

PART I-C (Concluded)

n	refers to condition at beginning of nozzle
p	refers to the initial propellant condition
t	refers to condition at nozzle throat
w	refers to the detonation wave
$\overline{f}$	denotes f/f_o

Note: Absence of subscript refers to the local condition in the chamber for the wave fixed system of coordinates.

FOREWORD

This report represents the Second Quarterly Progress Report, 1 September 1962, to 30 November 1962, on Contract No. AF 04(611)-8503, a contract between Edwards Air Force Base and The University of Michigan. The aim of this contract is to investigate the feasibility of a rotating detonation wave rocket motor.

Personnel associated with the various phases of the program as they are divided in the report are as follows:

I-A - J. Fu
B - M. Sichel, T. David
C - T. C. Adamson, G. Olsson

II-A - G. L. Cosens, J. Brown
B - G. L. Cosens, K. Ragland
C - G. L. Cosens, F. Cheslak, J. Brown
D - E. Kurath, S. Schmidt

This project is directed by Professors J. A. Nicholls and R. E. Cullen of The University of Michigan. The Air Force Project Engineer is Richard Weiss (DGRR), 6593d Test Group (Development), Edwards Air Force Base, California.

SUMMARY

This report presents the work accomplished on the rotating detonation wave engine feasibility program during the period 1 September 1962 to 30 November 1962.

The work described in this report represents the continuation of the experimental and theoretical studies that will consume approximately the first half of the program. The last half of the program will be devoted to the fabrication and testing of a nominal 1000 lb thrust H_2-O_2 rocket motor utilizing the detonative mode of combustion.

The theoretical studies have been continued in the two areas studied during the first quarter. In addition, the study of a third problem has been initiated.

(1) The study of the structure of a detonation wave through a two-phase medium has continued emphasizing the droplet shattering mechanism. Utilizing a theoretical relation for a shear-type breakup developed by Dodd, it is concluded that the distance predicted for droplet breakup behind the strong normal shock wave associated with an H_2-O_2 detonation can be much smaller than experimentally observed distances between the shock and the zone of significant chemical reaction. It is concluded therefore that the droplet shattering effect occurring behind the shock wave can be of extreme importance in substaining a Chapman-Jouguet detonation in dilute sprays.

(2) The study of the heat transfer to the wall of a rotating detonation wave engine has been continued. For the case of dissociative recombination at the wall, the conclusions are that the heat flux to the wall is increased about 35 percent over the case without dissociative recombination studied earlier. Curves are presented showing this effect as a function of the mole fraction of H_2 present in the unburned gases. The maximum heat flux occurs for a fuel-rich mixture of $X_{H_2} = 0.75$ (oxidizer to fuel weight ratio of 5.3). It is concluded also that according to the simplified model derived earlier, that the heat flux for the rotating detonation wave engine with dissociative recombination occurring still is of the same order as the heat flux at the throat of a small conventional H_2-O_2 rocket motor.

(3) The study of an analytical model for the gas dynamics associated with the rotating detonation wave engine has been initiated. Utilizing the basic assumptions that the flow is steady with respect to the detonation waves, and that the flow is quasi-one dimensional in the circumferential direction, the conservation equations lead in general to a system of first order, ordinary differential equations relating the flow properties in the chamber and a dimensionless circumferential distance, η. The case of instantaneous, complete mixing of the burned and unburned propellant is treated as well as the case of no mixing.

The experimental studies on all the phases reported during the first quarter are continuing.

(1) Instrumentation has been essentially completed on the 100 lb thrust motor and initial runs have been made. Due to difficulties with the miniature Kistler pressure transducer for recording chamber pressure in the engine as a function of time, the transducer has been installed in the straight detonation tube for shakedown and calibration utilizing a known wave form.

(2) The studies of the pressure and temperature effects on detonation velocities have progressed to the point of substantiating the data of Moyle down to 160°K at a pressure of one atmosphere. In subsequent tests, it appears that the coiled tube will have to be removed from the cooling bath and brought up to room temperature to eliminate the ice formation of the combustion products on tube walls between each run.

(3) Instrumentation of the condensation chamber for the study of droplet formation by rapid expansion and condensation is almost complete. The detonation tube has been fabricated for the study of detonating through droplet fields produced by either condensation or injection techniques.

(4) The geometrical tests performed to date have investigated the wave structure of detonations in a curved tube without side relief. It is concluded that a multiply-reflected wave occurs in the burned gases behind H_2-O_2 detonation waves in nearly stoichiometric mixtures. Also, the initial wave front is slightly inclined to the radial direction.

I. THEORETICAL STUDIES

A. DETONATION WAVE IN HETEROGENEOUS, LIQUID-GAS MEDIA

It was concluded in earlier studies[1] that the droplet shattering phenomenon could be of considerable importance in sustaining stable detonation waves through heterogeneous, liquid-gas media, where either the fuel or the oxidizer are initially in the form of a dilute spray of liquid droplets.

The following is a study utilizing the best theoretical and experimental information available to predict the order of the breakup times for relatively large (500 - 1000 μ) liquid-oxygen droplets subjected to the strong shock wave associated with a H_2-O_2 detonation.

1. Some Experimental Observations Concerning the Droplet Breakup Process

Experimental results[4-6] show that two types of droplet breakup exist in the zone behind a shock wave front: the bag-type breakup and the shear-type breakup. The successive stages of a droplet breakup process can be described phenomenalogically: (1) For a bag-type breakup, the increased pressure on the droplet surface, due to the high convective velocities following the wave front, flatten the droplet into a disk-shape, having its face perpendicular to the direction of the flow. Then the center portion is blown out into a thin hollow bag anchored to a heavy rim.* Finally the thin bag bursts into small droplets, while the rim breaks into fragments. Photographic evidence on this phenomenon appears in References 4 and 5. (2) For a shear-type breakup, in contrast, the droplet is distorted into a saucer-shaped disk with its convex surface facing to the gas flow. Then a thin ring layer is drawn out from the edges of the disk. Finally, the thin layer is stripped off the droplet and breaks up completely into micro-droplets. Engel[7] showed that the mechanism of micro-droplet formation is due to mechanical effects only and is not due to vaporization of liquid. Photographic details of this process may be found in References 5, 6, and 7.

2. Various Theories on Breakup of Droplets

However complex the phenomenon, it is highly desirable to treat it from both the experimental and theoretical aspects. The following is a discussion of pertinent theoretical analyses concerning the shattering processes of a droplet:

---

*Lane[5] states that up to 70 percent of the liquid remains in the rim.

a) Hinze's Theory.—One of the earliest mathematical analyses on this subject was presented by Hinze.[8] The theory is based on linearized hydrodynamical equations for slight deformations of a droplet in an air flow. The main emphasis was in the derivation of the relation between critical speed and critical size. Considering the influence of the aerodynamic-pressure on a droplet and the surface tension of the droplet, Hinze found the criterion for determining breakup of a droplet to be the relevant value of the Weber number. By using the experimental data of Merrigton and Richardson,[9] Hinze indicated the critical Weber number, $(We)_{cr} = 10$.* However, the critical Weber number can be derived theoretically by using the critical radius $(r)_{cr}$ [see Eq. (3) of Section b] and the definition of the Weber number. It shows the critical Weber number, $(We)_{cr} = 8$, which agrees closely with Hinze's value. Hinze also found that the effect of viscosity of liquid on deformation appears small except for large values of viscosity, e.g., viscosities of the order of glycerol. In this case, the viscosity effect tends to retard the breakup. The effect of viscosity on breakup has been studied in more detail by Hanson.[11] He found that when the viscosity of a liquid is less than about 10 centistokes, the effect on droplet breakup is negligible; while if it is between 10 and 100 centistokes, the breakup process is retarded.

b) Mathematical Model for Bag Type Breakup of a Droplet. This mathematical analysis was proposed by Gorden.[12] In the analysis, it is assumed that a cylindrical plug of diameter r and length 2r (where r is the radius of the droplet) is extruded from a droplet; while the rest of the droplet around the cylinder remains at rest. This deformation is caused by the air pressure in front of the droplet, but is retarded by surface tension, viscosity, and inertial forces of the droplet. Estimating the magnitude of the pressures caused by these forces, and combining them with the inertial effect, a differential equation for the extruded cylinder is obtained, i.e.,

$$\frac{dv}{dt} = \frac{1}{\rho_\ell D}\left(\frac{1}{2}\rho_g U^2 - \frac{16\,\mu_\ell\, v}{D} - \frac{8S}{D}\right) \tag{1}$$

where v = velocity of the extruded cylinder. Equation (1) is solved for the instantaneous velocity, v, and the resulting equation is in turn solved for the instantaneous displacement of the cylinder as a function of time. The displacement is then set equal to the droplet diameter D to determine the total breakup time, t_b. The result is:

$$\frac{2(16\mu_\ell)^2}{\rho_\ell D^2\left(\rho_g U^2 - \frac{16S}{D}\right)} = \frac{16\mu_\ell t_b}{\rho_\ell D^2} - 1 + \exp\left[\frac{-16\mu_\ell t_b}{\rho_\ell D^2}\right] \tag{2}$$

*Hinze[8] defined $We = (\rho_g U^2 r)/S$ but Williams[10] defined $We = [\rho_g U^2 (2r)]/S$. In this report, Hinze's definition will be adapted.

where t_b is the breakup time. The breakup time approaches infinity if a droplet is stable. Hence it is obvious from Equation (2) that the critical condition occurs at

$$\left(\rho_g U^2 - \frac{16S}{D}\right) = 0$$

which implies the critical radius is given by

$$(r)_{cr} = \frac{8S}{\rho_g U^2} \tag{3}$$

Equation (3) is formally identical with Lane's[5] empirical formula, which has been used in correlating experimental results[4,5] between critical speed and critical size. However, Equation (3) will be used in this report for the same purpose.

Since Equation (2) cannot be solved analytically for the breakup time, a useful approximate solution is

$$t_b = \frac{2D\rho_\ell^{1/2}}{\left(\rho_g U^2 - \frac{16S}{D}\right)^{1/2}} + \frac{32\,\mu_\ell}{\left(\rho_g U^2 - \frac{16S}{D}\right)} \tag{2-a}$$

Hanson[11] and co-worker showed experimentally that the effect on breakup can be neglected when the viscosity, $\mu_\ell \leq 10$ centistokes. For this case the bag-type breakup time is approximately

$$t_b = \frac{2D\,\rho_\ell^{1/2}}{\left(\rho_g U^2 - \frac{16S}{D}\right)^{1/2}} \tag{2-b}$$

It should be noted that according to this theory, Eq. (2-b) can predict the breakup time of droplets larger than critical size, and for droplets of critical sizes the breakup time is infinite.

c) Mathematical Model for Shear-Type Breakup of a Droplet.—This mathematical model is attributed to Dodd.[13] The basic considerations of this theory are as follows: The tangential frictional aerodynamic forces cause an internal circulation in the surface layer of a droplet. In turn, the centrifugal effect resulting from the circulation causes bulges to form on the surface. On the other hand, the surface tension of the droplet has a retarding effect on bulge formation. If the pressure due to the centrifugal effect equals a fraction, F, of the surface tension pressure, then breakup occurs. The assumptions used in Dodd's

analysis are: 1. The circulation velocity is uniform across the thin surface layer; 2. Inside the moving layer the liquid is at rest; 3. The frictional force on the surface of the droplet is equal to $0.332\sqrt{(U^3\mu_g\rho_g)/r}$ and this force acts over a region of length r (see Fig. 2 of Ref. 1); 4. The thickness of the moving layer is "fr"; where $0 < f < 1$. Based upon the balance of the energy transfer rate between the gas flow behind the shock front and the droplet, a breakup time for a droplet is derived:

$$t_b = \frac{2r}{(1.5U)^{3/2}} \frac{1}{0.332} \sqrt{\frac{S\rho_\ell}{\mu_g\rho_g}} \sqrt{\frac{F}{f}}$$

or

$$t_b = \frac{3.28r}{U^{3/2}} \sqrt{\frac{S\rho_\ell}{\mu_g\rho_g}} \sqrt{\frac{F}{f}}$$

By using Engel's[7] experimental data, with $\sqrt{F/f} = 0.5$.

$$t_b = \frac{1.64r}{U^{3/2}} \sqrt{\frac{S\rho_\ell}{\mu_g\rho_g}} \tag{4}$$

Due to the inequality of pressure on the upstream and downstream sides, each bulge is subjected to an aerodynamic drag tending to move the bulge off the surface of the droplet. Dodd[13] has pointed out that the effect of the aerodynamic force which reinforces the frictional force on the droplet surface, will decrease the breakup time. Therefore, the breakup time given by Eq. (4) is too high, and some modification factor is needed to give the correct breakup time. Inasmuch as Dodd did not attempt to evaluate this factor, an attempt will be made to estimate this factor approximately by comparing the order of magnitude of the aerodynamic force and the frictional force.

Let p = the aerodynamic pressure = $1/2\ \rho_g U^2$

p_f = the frictional force per unit area = $0.332\sqrt{(U^3\ \mu_g\rho_g)/r}$

$$\frac{p_f + p}{p_f} = 1 + \frac{p}{p_f} = 1 + \frac{1/2\ \rho_g\ U^2}{0.332\sqrt{\frac{U^3\mu_g\rho_g}{r}}}$$

$$= 1 + 1.5\sqrt{\frac{\rho_g U r}{\mu_g}} = 1 + 1.5\ \sqrt{Re}$$

$$\frac{p_f + p}{p_f} = 1 + 1.5\ \sqrt{Re}$$

Since the impulse on the droplet due to the gas is equal to product of the force and the time over which it acts, it implies the breakup time is inversely proportional to the force. Hence breakup time given by Eq. (4) should be modified by a factor $1/(1 + 1.5\sqrt{Re})$, i.e.,

$$t_b = \frac{1.64r}{U^{3/2}}\sqrt{\frac{S\rho_\ell}{\mu_g\rho_g}}\,\frac{1}{1 + 1.5\sqrt{Re}} \qquad (4\text{-a})$$

In investigating the disintegration of water drops in an air stream, where the relative velocity between air and the drop increases gradually, Dodd found the critical radius for a droplet is

$$(r)_{cr} = \frac{6.67S}{\rho_g\beta\, U^2}$$

where β is a correction factor $0 < \beta < 1$. Lane,[14] using Taylor's loading spring concept suggests that:

$$\frac{\text{Velocity for bursting by suddenly applied blast}}{\text{Velocity of bursting in steady stream}} = 0.71$$

In Reference 14, Lane found this factor agrees reasonably well with experimental data. Using this value, the correlation between critical relative velocity and critical size becomes

$$(r)_{cr} = 13S/(\rho_g U^2) \qquad (5)$$

3. Comparison Between Theories and Experiments

In order to estimate the validity of these mathematical models, some calculations have been made. The results are listed in Tables I, II, III, and IV. Since it has been pointed out by Rabin[6] that small droplets undergo a bag-type breakup while the large droplets experience a shear-type breakup, Eq. (3) is used to correlate the critical conditions for small droplets, while Eq. (5) is used for large droplets. When applying Gorden's correlation, Eq. (3), to the experimental data, in Reference 6, for $(r)_{cr} = 500\ \mu$, the deviation between theoretical and experimental critical radii is over 50 percent. It is felt that Eq. (3) is valid only for $r < 500\mu$, while Eq. (5) applied for $r > 500\ \mu$.

Equation (4-a) gives the breakup time for the shear-type breakup for droplets of critical size as well as for droplets larger than critical size. Some calculated results, by using Equation (4-a) and the experimental data given by Reference

(6) are listed in Table III. It indicates the breakup time for droplets of r - 500 μ and relative air flow velocities of the range 55 ft/sec < U < 93 ft/sec, is about 1 millisecond. The velocities used in the above experiments were much lower in comparison to the velocity occurring behind the strong normal shock wave associated with the detonation process. Hence, the breakup time in the zone behind the detonation wave front would be expected to be much smaller than the values listed in Table III. In order to estimate the order of the droplet breakup time in the detonation case, the following analysis is made utilizing Equation (4-a) and the detonation characteristics of hydrogen-oxygen mixtures calculated by Moyle.[15] For a mixture having a mole fraction of 0.667 hydrogen, a detonation velocity of about 9400 ft/sec is obtained. Assuming that the structure of a spray detonation consists of a normal shock wave followed by combustion, the gas velocity immediately behind the normal shock front is supersonic and causes a detached shock wave in front of the droplet. It is the gas flow behind the detached shock that is responsible for droplet breakup. Using the conservative minimum value of the sub-sonic velocity behind the detached shock, the breakup time for oxygen droplets having a size range of $500 \leq r \leq 1000$ μ have been calculated. The results are shown in Table IV. The breakup times are in order of 0.1 μ-sec. In this time interval the detonation wave front will travel a distance approximately equal to 1×10^{-2} in. This distance will be denoted by L_B. Morrison[16] has found from schlieren photographs utilizing fuel-lean gaseous mixtures that there can be a measurable distance between the leading shock wave front and the zone where significant chemical reaction takes place. Under these conditions, detonation waves propagating at velocities in good agreement with velocities calculated for Chapman-Jouguet detonation waves give evidence that this zone may be as great as two tube diameters or more in a 0.5 in. diameter tube. Denoting this distance by L_C, it follows that for H_2-O_2 detonations in lean gaseous mixtures $L_C = O(1)$ and therefore $L_B \ll L_C$.

4. Conclusions

The Weber number appears to be an important criterion concerning the droplet-shattering phenomenon. Hinze has shown there exists a critical Weber number of a dilute spray, $(We)_{cr} = 10$. When the Weber number is larger than this value, the droplets tend to break up.

Utilizing a theoretical relation developed by Dodd, the breakup times for oxygen droplets in a H_2-O_2 spray detonation have been calculated. For oxygen droplets within a size range of $500 \leq r \leq 1000$ μ, the breakup time is of the order of 0.1 μsec. In this time interval the detonation wave front will travel a length, $L_B = 1 \times 10^{-2}$ in. In comparing this order of L_B, with the order of L_C, the length between the shock wave front and the zone of significant chemical reaction, it follows that $L_B << L_C$. Thus it is indicated that large droplets will be shattered into microdroplets in a zone sufficiently small behind the shock wave front, that if the subsequent evaporation and combustion of these microdroplets occur rapidly enough, a heat release sufficient to sustain a Chapman-Jouguet detonation wave is possible. Thus it appears that the droplet

breakup processes occurring behind the shock wave can be an important mechanism in stabilizing a detonation wave in a dilute spray.

It is obvious that experimental results substantiating these theoretically predicted droplet breakup times behind strong shock waves is highly desirable.

B. STUDY OF HEAT TRANSFER IN THE ROTATING DETONATION WAVE ENGINE

The work described below is a continuation of the heat transfer study, which was presented in detail in Reference 1. The effects of dissociation and recombination and of fuel-oxidizer mixture ratio upon the heat transfer have been investigated. As mentioned in Reference 1, the recombination of dissociated species which are present behind the detonation can result in an appreciable increase in the heat flux across the boundary layer.

In a dissociating gas, energy is transported not only by conduction but also by the diffusion of atomic species. The heat flux across a boundary layer in a dissociated gas may be increased by the recombination of atomic species within the boundary layer and by diffusion of atomic species from the free stream to the cold wall where, in most cases, recombination with heat release occurs. When the Lewis number, $Le = (C_p D\rho)/k$, is unity the heat transfer across a boundary layer in contact with a cold, catalytic wall is proportional to the difference between the free stream and wall enthalpies regardless of the energy transfer mechanism.[17] The enthalpy of course must include the chemical heat of formation.

For a preliminary estimate of the increase in heat transfer due to dissociation it has been assumed that $Le = 1.0$. Consequently it has been possible to use the boundary layer heat flux results of Reference 1, the only change being in the calculation of the enthalpy difference across the boundary layer.

The heat flux to the wall also depends upon the ratio of hydrogen to oxygen in the explosive mixture into which the detonation propagates. Consequently, calculations of wall heat flux have been made for $0.40 \leq X_{H_2} \leq 0.80$ where X_{H_2} is the mole fraction of molecular hydrogen. The composition of the combustion products at the Chapman-Jouguet plane have been computed by Moyle,[15] and his results, which were used in the calculations, are reproduced in Fig. 1.

The heat flux was computed as described in Reference 1, i.e.

$$q_w = \frac{(h_r - h_w)\tau_w}{(V_D - V_e)Pr_m^{2/3}} \qquad (1)$$

where τ_w, the shear stress at the wall is given by Equation (9) in Reference 1.

$$\frac{\tau_w}{\rho_e V_e^2} = .0460 \left(\frac{\theta}{\delta}\right) \left[\phi \left(1 - \frac{V_D}{V_e}\right) \frac{\delta}{\theta} \right]^{4/5} \left(\frac{V_D}{V_e} - 1\right)^{3/5} \left(\frac{\nu_e}{V_e}\right)^{1/5} \left(\frac{1}{x}\right)^{1/5}$$

where

$$\phi = \left(\frac{\mu_m}{\mu_e}\right)^{1/4} \left(\frac{\rho_m}{\rho_e}\right)^{3/4}$$

and where the subscript m indicates that ρ and μ are calculated at the temperature corresponding to the Eckert reference enthalpy

$$h_m = 0.5 (h_w + h_e) + 0.22 (h_r - h_e) \tag{2}$$

The free stream enthalpy per unit mass of gas consisting of the constituents of the equilibrium mixture at the Chapman-Jouguet plane was computed according to the equation

$$h = \frac{1}{\overline{W}} \sum_{i=1}^{n} X_i [H_{i,T_e} - H_{i,298.16^\circ K} + \Delta H^\circ_{f_i}] \tag{3}$$

where $\overline{W}$ is the average molecular weight of the mixture given by

$$\overline{W} = \sum X_i W_i \tag{4}$$

the enthalpies and standard heats of formation have been taken from the tables in Penner.[18] The recovery enthalpy of the turbulent boundary layer was once again computed according to

$$h_r = h_e + \left(\frac{V_D}{V_e} - 1\right)^2 \frac{V_e^2}{2} (Pr_m)^{1/3} \tag{5}$$

In computing the reference temperature from h_m it was assumed that the fluid composition was the same as in the free stream. The validity of this assumption is somewhat questionable and must be studied further.

A wall temperature of 900° R was assumed. Since dissociation is negligible at this temperature the gas at the wall will consist of H_2 and H_2O for the rich mixtures and O_2 and H_2O for the lean mixtures.

The results of the calculations described above are presented in Table V and in Fig. 2. It can be seen that the heat flux values computed by taking dissociation into account are about 35% more than the non-dissociative value. The maximum heat flux occurs for a fuel-rich mixture with $X_{H_2} = 0.75$ or a ratio

of oxidant to fuel weight of 5.3. Again assuming as in Reference 1 that the heat pulse lasts for only one third of the period between the passage of successive waves, the maximum value of the overall heat flux, $\bar{Q}_w$, to the walls of the 100-lb thrust engine at $X_{H_2} = 0.75$ becomes

$$\bar{Q}_w\Big|_{max} = 1660 \text{ Btu/ft}^2 \text{ sec} = 11.5 \text{ Btu/in.}^2 \text{ sec}$$

For the mixture with $X_{H_2} = 0\ 60$, which was considered in Reference 1 the overall heat flux density would be

$$\bar{Q}_w\Big|_{X_{H_2} = 0.60} = 1480 \text{ Btu/ft}^2 \text{ sec} = 10.2 \text{ Btu/in.}^2 \text{ sec}$$

It is interesting to compare the above values of $\bar{Q}_w$ to the nozzle throat heat flux of 9.95 Btu/in.^{2} sec computed by Curran et al[19] for a conventional H_2-O_2, 1000-lb thrust rocket for a mixture with $X_{H_2} = 0.84$ (corresponding to maximum specific impulse). Thus the heat flux of the 100-lb rotating detonation wave engine is of the same order as the throat heat flux of a small conventional engine, and this is still in essential agreement with the conclusion reached in Reference 1.

Nevertheless, the calculations above indicate basic differences between the rotating detonation wave and conventional rocket motors. For a given mixture ratio the temperature behind a detonation is higher than in a conventional combustion chamber with a corresponding increase in the dissociation of the combustion products. This can be seen from Fig. 3 which shows the variation of T_e, the temperature behind the detonation and T_c, the temperature in a conventional 300 psia combustion chamber[20] with X_{H_2}. At the mixture ratio for which Isp, the specific impulse of a conventional engine is a maximum, T_c is about 1000°F lower than T_e. The dissociation behind the detonation is thus sufficient to cause an appreciable increase in the heat flux, as is shown by the calculations above. Even though the temperature T_e, reaches a maximum value near the stoichiometric composition with $X_{H_2} = 0.667$, the velocity difference, $(V_D - V_e)$, across the wave continues to increase as X_{H_2} increases. Since heat flux increases with both $(V_D - V_e)$, and $(h_r - h_w)$, the maximum heat flux occurs with a rich mixture, $X_{H_2} = 0.75$, rather than occurring near the stoichiometric mixture ratio, $X_{H_2} = 0.667$.

C. ESTABLISHMENT OF AN ANALYTICAL MODEL OF THE ROTATING DETONATION WAVE ENGINE*

1. Introduction

It is highly desirable to be able to establish the effects of the various design parameters (engine sizing, flow rate of propellants, etc.) on the theoretical performance of the rotating detonation wave engine. To accomplish this it is necessary to formulate an analytical model of the engine. This model, while retaining the essential physical features, should be simple enough to permit insight into the gasdynamics of engine operation. Also, the results of the analysis should correlate with data from the experimental engine tests. Once a reasonable analytical model is established it can be used as a design tool and as a basis for comparing the theoretical performance of the rotating detonation wave engine with that of other types of propulsion devices.

The fluid flow field in the engine is three dimensional and unsteady with heat and mass addition and turbulent mixing taking place. As a result, simplifying assumptions must be made to achieve a solvable mathematical model. The key assumption is that the detonation wave velocity is constant, so that the fluid flow field is steady and quasi-one dimensional with respect to the detonation waves. Both the burned and unburned propellants are treated as ideal gases and the effects of shear forces and heat transfer on the flow are neglected. These restrictions provide the basis for a simplified analytical model of the engine. The effects due to the turbulent mixing of the burned and unburned propellants are to be estimated by considering alternatively the limiting cases of instantaneous complete mixing and of no mixing.

2. Fundamental Assumptions and Conditions

Because of the complex nature of the gasdynamics of the rotating wave engine it is necessary to impose restrictive assumptions to establish a reasonable mathematical model. The following is a presentation of these assumptions with remarks concerning their validity.

(a) The fluid flow field in the engine is assumed to be steady and quasi-one dimensional with respect to the moving detonation waves.

The necessary conditions implied in this assumption are:

(1) The detonation wave speed has reached a steady state, constant value.

(2) The chamber dimensions are small compared to the radius of curvature

*This analysis is largely the effort of T. C. Adamson, Professor of Aeronautical and Astronautical Engineering at The University of Michigan. The authors are extremely grateful for this contribution.

of the chamber centerline.

(3) The chamber fluid properties vary only in the circumferential direction.

(4) In the chamber the velocity in the axial direction is small compared to the velocity in the radial direction.

Order of magnitude condition for the radial pressure variation in the chamber to be small:

For a curved streamline

$$\frac{dP}{dn} = \frac{1}{R} \rho V_a^2$$

In order to have a negligible pressure variation in the radial direction,

$$\frac{dP}{dn} \ll \frac{P}{\ell_c}$$

Hence,

$$\frac{\ell_c}{R} \ll \frac{P}{\rho V_a^2}$$

But,

$$\frac{P}{\rho V_a^2} = \frac{1}{\gamma M_a^2}$$

which is of order one. Then the condition for the radial pressure variation to be small is

$$\frac{\ell_c}{R} \ll 1$$

Order of magnitude condition for the unsteady fluctuation of pressure in the chamber to be small:

The time for an acoustic wave to cross the chamber in the axial direction must be much less than the time the detonation wave takes to travel the distance between successive waves. Therefore, the condition is,

$$\frac{x_n}{a} \ll \frac{2\pi R}{N V_w}$$

or

$$\frac{x_n}{R} \ll \frac{2\pi a}{NV_w}$$

The minimum value of a is a_1 and since

$$\frac{V_w}{a_1} = M_w$$

The condition becomes

$$\frac{x_n}{R} \ll \frac{2\pi}{NM_w}$$

M_w is of the same order as 2π and N is of the order one. Then the condition for negligible axial unsteady fluctuation of pressure in the axial direction is

$$\frac{x_n}{R} \ll 1$$

For a given engine geometry these comparisons can be used to check the assumption of one dimensional flow.

(b) The fluid flow through the convergent section of the nozzle is assumed to be quasi-one dimensional in the axial direction.

As a consequence, the axial component of velocity at the throat is equated to the local speed of sound and the circumferential velocity component is assumed to be invariant with respect to the axial direction.

(c) It is assumed that the detonation wave is a plane discontinuity.

The detailed structure of the detonation wave is not to be considered. It is to be treated hydrodynamically as a shock wave with heat addition.

(d) Both the burned and unburned propellants are assumed to be ideal gases.

The influences of the variation of gas parameters with temperature and pressure are to be neglected and all chemical reaction is assumed to take place only at the detonation wave.

(e) Shear forces and heat transfer effects are to be neglected.

(f) The propellant mass flow rate through the injector is assumed to be constant and uniform in distribution.

Assuming the propellants are delivered to the injector in the gaseous state, this condition is satisfied if the injector to chamber pressure ratio is always at or above the critical value and if the injector design is axially symmetric.

In order to derive the conservation equations (continuity, momentum, and energy) two special cases are designated. In the first case the burned and unburned gases are treated as being completely mixed, and in the second case the gases are treated as being unmixed. It is believed that this approach will give some insight into the effect of mixing on the performance of the engine.

3. Definition of Coordinate Systems

Because the radial width is considered to be small compared to the radius of curvature, the chamber can be "unrolled" and stretched out. Then the problem is one wherein a long tube of constant cross-sectional area has unburned mass entering on one side and burned mass being ejected on the other. In this tube detonation waves occur periodically a distance L apart, each moving at a constant velocity, V_w. From the viewpoint of an observer on any wave the problem becomes steady and periodic.

The Wall Fixed System:

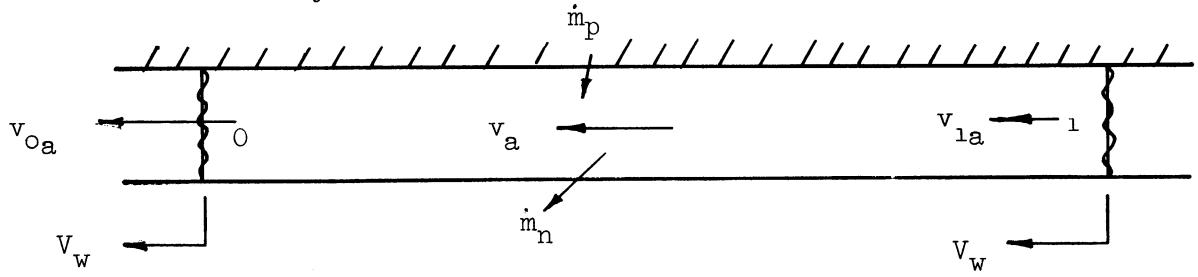

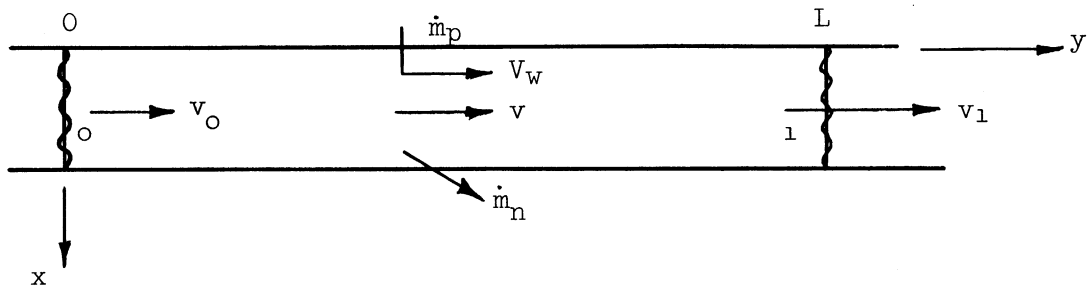

Note: Arrows define the direction of positive velocity.

The two systems are related by the transformations

$$v = V_w - v_a$$

$$y = V_w t$$

where t = 0 immediately after a wave passes.

4. Jump Conditions Across the Detonation Waves

The fluid flow properties at y = 0 and y = L are related by the hydrodynamic jump conditions across the detonation wave:

$$\rho_1 v_1 = \rho_o v_o$$

$$P_1 + \rho_1 v_1^2 = P_o + \rho_o v_o^2$$

$$C_{p_1} T_1 + \frac{1}{2} v_1^2 + \mu_1 Q = C_{p_o} T_o + \frac{1}{2} v_o^2$$

With the ideal gas assumption the thermal and caloric equations of state are,

$$P = \rho \frac{R_o}{\bar{m}} T$$

$$C_p T = \frac{\gamma}{\gamma - 1} \frac{R_o T}{\bar{m}}$$

and the speed of sound is given by

$$a^2 = \frac{\gamma P}{\rho}$$

The jump conditions can be expressed in the non-dimensional form

$$\bar{\rho}_1 \bar{v}_1 = 1$$

$$\bar{P}_1 + \gamma_o \bar{\rho}_1 \bar{v}_1^2 M_o^2 = 1 + \gamma_o M_o^2$$

$$\bar{C}_{p_1} \bar{T}_1 + \frac{\gamma_o - 1}{2} \bar{v}_1^2 M_o^2 + \mu_1 \bar{Q} = 1 + \frac{\gamma_o - 1}{2} M_o^2$$

$$\bar{P}_1 = \frac{\bar{m}_o}{\bar{m}_1} \bar{\rho}_1 \bar{T}_1$$

$$\bar{C}_{p_1} \bar{T}_1 = \frac{\gamma_o - 1}{\gamma_1 - 1} \bar{a}_1^2$$

$$\bar{a}_1^2 = \frac{\gamma_1}{\gamma_o} \frac{\bar{P}_1}{\bar{\rho}_1}$$

These equations may be solved to give $\bar{P}_1, \bar{v}_1$, etc. in terms of M_o and $\bar{Q}$. For example,

$$\bar{v}_1 = b + \sqrt{b^2 + c}$$

where b and c are defined by

$$b = \frac{\gamma_1}{\gamma_o}\left[\frac{1 + \gamma_o M_o^2}{(\gamma_1 + 1)M_o^2}\right]$$

$$c = \frac{2}{\gamma_o - 1}\left(\frac{\gamma_1 - 1}{\gamma_1 + 1}\right)\frac{1}{M_o^2}\left[\mu_1\bar{Q} - \frac{\gamma_o - 1}{2}M_o^2 - 1\right]$$

If $M_o = 1$ and $\gamma_1 = \gamma_o = \gamma$ this becomes

$$\bar{v}_1 = 1 + \sqrt{\frac{2\mu_1\bar{Q}}{\gamma + 1}}$$

In terms of $\bar{v}_1$,

$$\bar{P}_1 = 1 - \gamma_o M_o^2(\bar{v}_1 - 1)$$

$$\bar{a}_1^2 = \frac{\gamma_1}{\gamma_o}[1 - \gamma_o M_o^2(\bar{v}_1 - 1)]\bar{v}_1$$

5. Equations for the Case of Complete Mixing of the Burned and Unburned Propellant

In this case it is assumed that the burned and unburned gases mix completely and instantaneously and that the specific heat ratios and the molecular weights have one average value.

Choose a small increment of tube, of length dy, and write the conservation equations for two control volumes: one bounded by the chamber and the second bounded by the convergent section of the nozzle. In deriving the functional relations for the chamber conditions it is not necessary to consider the divergent section of the nozzle. This aspect is to be included in the evaluation of the thrust and the specific impulse of the engine.

Definition of Control Volumes:

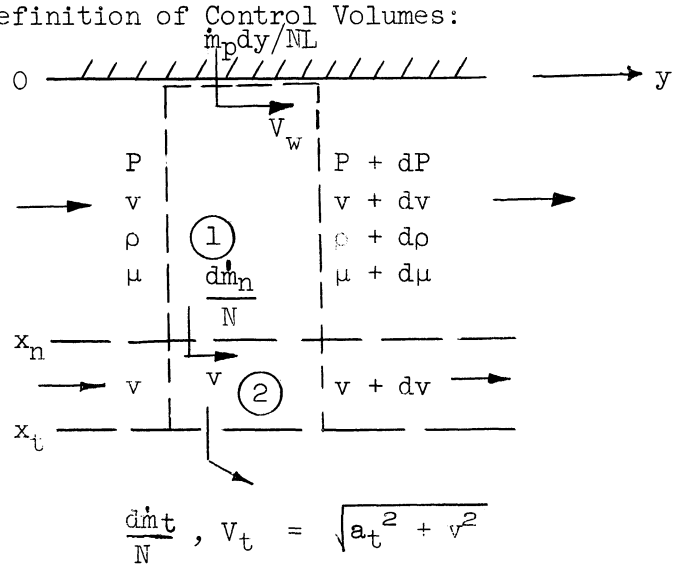

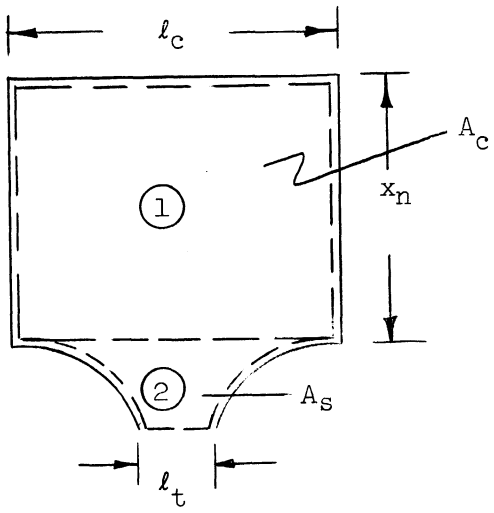

Equations for control volume (1)

Continuity Equation in (1)

$$\rho v A_c + \frac{\dot{m}_p}{NL} dy = (\rho + d\rho)(v + dv)A_c + \frac{d\dot{m}_n}{N}$$

$$d(\rho v A_c) = \frac{\dot{m}_p}{NL} dy - \frac{d\dot{m}_n}{N}$$

Continuity of the Unburned Species in (1)

$$(\rho v A_c)\mu + \frac{\dot{m}_p}{NL} dy = (\rho + d\rho)(v + dv)A_c(\mu + d\mu) + \frac{d\dot{m}_n}{N}\mu$$

$$d(\rho v A_c \mu) = \frac{\dot{m}_p}{NL} dy - \frac{d\dot{m}_n}{N}\mu$$

Combination with the continuity equation yields

$$\rho v A_c d\mu = (1 - \mu)\frac{\dot{m}_p}{NL} dy$$

y-Component of Momentum Equation in (1)

$$-\rho v^2 A_c - \frac{\dot{m}_p}{NL} V_w \, dy + v \frac{d\dot{m}_n}{N} + (\rho + d\rho)(v + dv)^2 A_c$$

$$= PA_c - (P + dP) A_c$$

$$d(\rho v^2 A_c) + A_c \, dP = \frac{\dot{m}_p}{NL} V_w \, dy - v \frac{dm_n}{N}$$

Combination of this with the continuity equation gives,

$$\rho v \, A_c \, dv + A_c \, dP = \frac{m_p}{NL} (V_w - v) \, dy$$

Energy Equation in (1)

$$\rho v \, A_c (h + \frac{1}{2} v^2) + \frac{\dot{m}_p}{NL} (h_p + \frac{1}{2} V_w^2) \, dy$$

$$= (\rho + d\rho)(v + dv) A_c [h + dh + \frac{1}{2} (v + dv)^2] + \frac{d\dot{m}_n}{N} (h + \frac{1}{2} v^2)$$

$$d[\rho v A_c (h + \frac{1}{2} v^2)] = \frac{\dot{m}_p}{NL} (h_p + \frac{1}{2} V_w^2) - \frac{d\dot{m}_n}{N} (h + \frac{1}{2} v^2)$$

Combining this with the continuity equation results in

$$\rho v A_c \, d(h + \frac{1}{2} v^2) = \frac{\dot{m}_p}{NL} (h_p + \frac{1}{2} V_w^2 - h - \frac{1}{2} v^2) \, dy$$

For a mixture of unburned and burned propellant the enthalpy is given by

$$h = \mu h_A + (1 - \mu) h_B$$

$$= \mu \left[\int_o^T C_{P_A} \, dT + h_A^{(o)} \right] + (1 - \mu) \left[\int_o^T C_{P_B} \, dT + h_B^{(o)} \right]$$

$$= C_p T + \mu h_A^{(o)} + (1 - \mu) h_B^{(o)}$$

since it has been assumed that $C_{P_A} = C_{P_B} = C_p$ = constant.

Now Q is defined by the relation,

$$h_A^{(o)} = Q + h_B^{(o)}$$

Therefore, the enthalpy is given by

$$h = C_p T + \mu Q + h_B^{(o)}$$

and the energy equation can be written as

$$\rho v A_c d(C_p T + \mu Q + h_B^{(o)} + \frac{1}{2} v^2) = \frac{\dot{m}_p dy}{NL} (C_p T_p + Q + h_B^{(o)} + \frac{1}{2} V_w^2 - C_p T - \mu Q - h_B^{(o)} - \frac{1}{2} v^2)$$

Combination with the continuity of species relation gives

$$\rho v A_c d(C_p T + \frac{1}{2} v^2) = \frac{\dot{m}_p dy}{NL} (C_p T_p + \frac{1}{2} V_w^2 - C_p T - \frac{1}{2} v^2)$$

Equations for control volume (2) :

Continuity Equation in (2)

$$\int_{A_s} \int \rho v dA_s + \frac{d\dot{m}_n}{N} = \int_{A_s} \int (\rho + dp)(v + dv) dA_s + \frac{d\dot{m}_t}{N}$$

$$d \int_{A_s} \int \rho v dA_s = \frac{d\dot{m}_n}{N} - \frac{d\dot{m}_t}{N}$$

Since it is assumed that the fluid flow in control volume (2) is quasi-one dimensional in the axial direction it is clear that the following inequality must be satisfied,

$$\frac{d \left[\int_{A_s} \int \rho v dA_s \right]}{d\dot{m}_t / N} \ll 1$$

This condition can be checked when a solution to the equations is obtained. Then the continuity equation becomes

$$d\dot{m}_n = d\dot{m}_t$$

Energy Equation in (2)

$$\iint_{A_s} \rho v(h + \frac{1}{2} V^2) dA_s + \frac{d\dot{m}_n}{N} (h + \frac{1}{2} v^2)$$

$$= \iint_{A_s} (p + d\rho)(v + dv)[h + dh + \frac{1}{2} (V + dV)^2] dA_s + \frac{d\dot{m}_t}{N} (h_t + \frac{1}{2} V_t^2)$$

$$d \iint_{A_s} \rho v(h + \frac{1}{2} V^2) dA_s = \frac{d\dot{m}_n}{N} (h + \frac{1}{2} v^2) - \frac{d\dot{m}_t}{N} (h_t + \frac{1}{2} V_t^2)$$

Again, it is assumed that

$$\frac{d \iint_{A_s} \rho v(h + \frac{1}{2} V^2) dA_s}{\frac{d\dot{m}_t}{N} (h_t + \frac{1}{2} V_t^2)} \ll 1$$

Obtaining as a result

$$\frac{d\dot{m}_n}{N} (h + \frac{1}{2} v^2) = \frac{d\dot{m}_t}{N} (h_t + \frac{1}{2} V_t^2)$$

which becomes

$$C_p T_t + \mu Q + h_B^{(o)} + \frac{1}{2} (a_t^2 + v^2) = C_p T + \mu Q + h_B^{(o)} + \frac{1}{2} v^2$$

or

$$a_t^2 = \frac{2}{\gamma + 1} a^2$$

The incremental mass flow out of the throat is given by

$$\frac{d\dot{m}_t}{N} = \rho_t a_t \ell_t dy$$

and since it is consistent with the assumptions to regard the fluid flow in the control volume (2) as being isentropic,

$$\frac{d\dot{m}_t}{N} = \rho a \left(\frac{2}{\gamma + 1}\right)^{\frac{\gamma + 1}{2(\gamma - 1)}} \ell_t dy$$

Therefore, the equations governing the flow in control volume (1) may be written as

$$d(\rho v A_c) = \left[\frac{\dot{m}_p}{NL} - \rho a \left(\frac{2}{\gamma + 1}\right)^{\frac{\gamma + 1}{2(\gamma - 1)}} \ell_t\right] dy$$

$$\rho v A_c d\mu = (1 - \mu) \frac{\dot{m}_p}{NL} dy$$

$$\rho v A_c dv + A_c dP = \frac{\dot{m}_p}{NL} (V_w - v)\, dy$$

$$\rho v A_c d(C_p T + \frac{1}{2} v^2) = \frac{\dot{m}_p}{NL} (C_p T_p + \frac{1}{2} V_w^2 - C_p T - \frac{1}{2} v^2) dy$$

$$P = \rho \frac{R_o}{\bar{m}} T$$

$$C_p T = \frac{a^2}{\gamma - 1}$$

$$a^2 = \frac{\gamma P}{\rho}$$

In non-dimensional form the equations become

$$d(\bar{\rho}\bar{v}) = (G - \frac{B}{M_o} \frac{\bar{P}}{\bar{a}}) d\eta$$

$$\bar{\rho}\bar{v} d\mu = (1 - \mu) G d\eta$$

$$\bar{\rho}\bar{v} d\bar{v} + \frac{1}{\gamma M_o^2} d\bar{P} = G(V_w - \bar{v}) d\eta$$

$$\bar{\rho}\bar{v} d(\bar{T} + \frac{\gamma - 1}{2} M_o^2 \bar{v}^2) = G(\bar{T}_p + \frac{\gamma - 1}{2} M_o V_w^2 - \bar{T} - \frac{\gamma - 1}{2} M_o^2 \bar{v}^2) d\eta$$

$$\bar{P} = \bar{\rho}\,\bar{T}$$

$$\bar{T} = \bar{a}^2$$

$$\bar{a}^2 = \bar{P}/\bar{\rho}$$

with the definitions,

$$G = \frac{\dot{m}_p}{\rho_o v_o A_c N}$$

$$B = \frac{2}{(\gamma + 1)} \frac{\gamma + 1}{2(\gamma - 1)} \frac{\ell_t L}{A_c}$$

$$\bar{T}_p = \frac{T_p}{T_o}$$

If $\bar{P}$, $\bar{v}$, $\bar{a}$, and μ are chosen to be the dependent variables one can write the equations in the form,

$$0 + 0 + 0 + \left(\frac{\bar{P}\bar{v}}{\bar{a}^2}\right)\frac{d\mu}{d\eta} = (1 - \mu)G$$

$$\left(\frac{\bar{v}}{\bar{a}^2}\right)\frac{d\bar{P}}{d\eta} + \left(\frac{\bar{P}}{\bar{a}^2}\right)\frac{d\bar{v}}{d\eta} - \left(\frac{2\bar{P}\bar{v}}{\bar{a}^3}\right)\frac{d\bar{a}}{d\eta} + 0 = G - \frac{B\bar{P}}{M_o\bar{a}}$$

$$\left(\frac{1}{\gamma M_o^2}\right)\frac{d\bar{P}}{d\eta} + \left(\frac{\bar{P}\bar{v}}{\bar{a}^2}\right)\frac{d\bar{v}}{d\eta} + 0 + 0 = G(\bar{V}_w - \bar{v})$$

$$0 + \left(\frac{(\gamma - 1)M_o^2\bar{P}\bar{v}}{\bar{a}^2}\right)\frac{d\bar{v}}{d\eta} + \left(\frac{2\bar{P}\bar{v}}{\bar{a}}\right)\frac{d\bar{a}}{d\eta} + 0 = G\left(\bar{T}_p + \frac{\gamma - 1}{2}M_o^2\bar{V}_w^2 - \bar{a}^2 - \frac{\gamma - 1}{2}M_o^2\bar{v}^2\right)$$

The determinant of the coefficients is given by

$$D = \begin{vmatrix} 0 & 0 & 0 & \frac{\bar{P}\bar{v}}{\bar{a}^2} \\ \frac{\bar{v}}{\bar{a}^2} & \frac{\bar{P}}{\bar{a}^2} & -\frac{2\bar{P}\bar{v}}{\bar{a}^3} & 0 \\ \frac{1}{\gamma M_o^2} & \frac{\bar{P}\bar{v}}{\bar{a}^2} & 0 & 0 \\ 0 & \frac{(\gamma - 1)M_o^2\bar{P}\bar{v}^2}{\bar{a}^2} & \frac{2\bar{P}\bar{v}}{\bar{a}} & 0 \end{vmatrix}$$

$$D = \frac{2\bar{P}^3\bar{v}^2}{\gamma M_o^2 \bar{a}^5}(1 - M^2)$$

To complete the statement of the problem for the complete mixing case it is necessary to specify the end conditions. At $\eta = 0$ by definition,

$$\bar{P}_o = \bar{v}_o = \bar{a}_o = 1, \quad \mu_o = 0$$

and at $\eta = 1$ the jump conditions across the detonation wave give the relations,

$$\bar{v}_1 = b + \sqrt{b^2 + c}$$

$$\bar{P}_1 = 1 - \gamma M_o^2(\bar{v}_1 - 1)$$

$$\bar{a}_1 = \sqrt{[1 + \gamma M_o^2(1 - \bar{v}_1)]\bar{v}_1}$$

where b and c reduce to,

$$b = \frac{1 + \gamma M_o^2}{(\gamma + 1)M_o^2}$$

$$c = \frac{2}{(\gamma + 1)M_o^2}\left[\mu_1\bar{Q} - \frac{\gamma - 1}{2}M_o^2 - 1\right]$$

6. Equations for the Case of No Mixing of the Burned and Unburned Propellant

Here it is assumed that the burned and unburned gases are separated by an interface which is stationary with respect to the moving waves and across which no mass or energy transfers. The burned and unburned gases are assumed to have distinct values of specific heat ratios and molecular weights, namely, γ_B, γ_A, $\bar{m}_B$ and $\bar{m}_A$. In other respects the treatment follows that of the complete mixing

case. Control volume (1) is split by the interface into two sections, A and B corresponding to the unburned and the burned propellants, respectively. In each section the flow is assumed to be quasi-one dimensional in the circumerential direction. The pressure gradient across the interface is taken to be zero. The slope of the interface is assumed to be small. Since the slope of the interface is given by

$$\frac{dx}{dy} = \frac{u}{V}$$

i.e., the interface must be a streamline. This assumption is consistent with the previous condition

$$\frac{u}{V} \ll 1$$

The treatment of control volume (2) is identical to that of the complete mixing case, and the results can be stated as

$$\dot{dm}_n = \dot{dm}_t$$

$$\frac{\dot{dm}_t}{N} = \rho_B a_B \left(\frac{2}{\gamma_B + 1}\right)^{\frac{\gamma_B + 1}{2(\gamma_B - 1)}} \ell_t \, dy$$

Definition of control volumes:

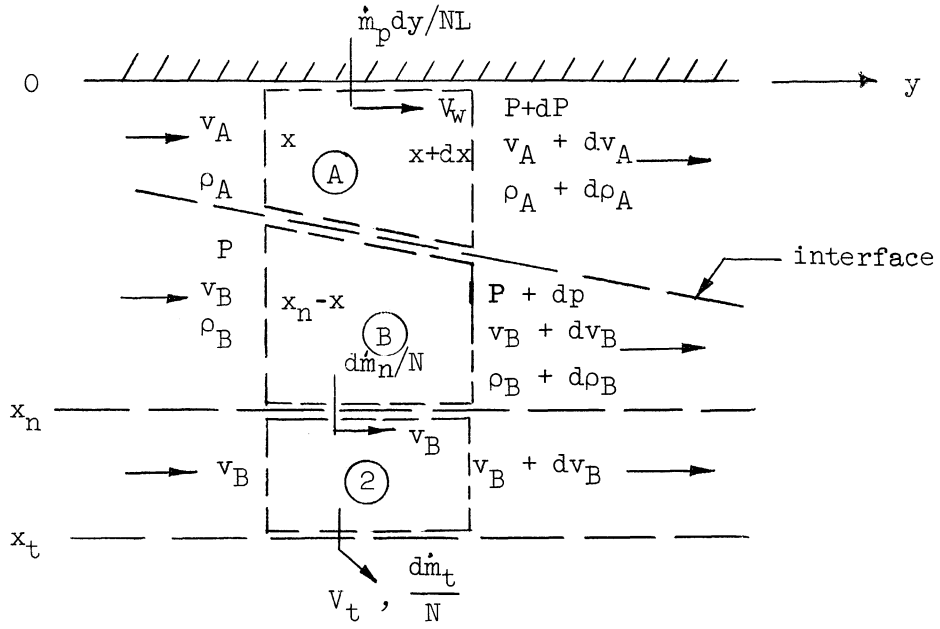

Equations for control volume (A):

Continuity Equation in (A)

$$\rho_A v_A \ell_c x + \frac{\dot{m}_p}{NL} dy = (\rho_A + d\rho_A)(v_A + dv_A)\ell_c(x + dx)$$

$$d(\rho_A v_A \ell_c x) = \frac{\dot{m}_p}{NL} dy$$

Upon integration this becomes, since $x = 0$ when $y = 0$,

$$\rho_A v_A \ell_c x = \frac{\dot{m}_p}{NL} y$$

y-Component of the Momentum Equation in (A)

$$- \rho_A v_A^2 \ell_c x - \frac{\dot{m}_p}{NL} V_w dy + (\rho_A + d\rho_A)(v_A + dv_A)^2 \ell_c(x + dx)$$

$$= P\ell_c x - (P + dP)\ell_c(x + dx) + P\ell_c dx$$

$$d(\rho_A v_A^2 \ell_c x) + \ell_c x dP = \frac{\dot{m}_p}{NL} V_w dy$$

Combination with the continuity equation gives

$$\frac{\dot{m}_p}{NL} y\, dv_A + \ell_c x dP = \frac{\dot{m}_p}{NL} (V_w - v_A) dy$$

Energy Equation in (A)

$$\rho_A v_A \ell_c x(h_A + \tfrac{1}{2} v_A^2) + \frac{\dot{m}_p}{NL} (h_p + \tfrac{1}{2} V_w^2) dy$$

$$= (\rho_A + d\rho_A)(v_A + dv_A)\ell_c(x + dx)[h_A + dh_A + \tfrac{1}{2}(v_A + dv_A)^2]$$

$$d[\rho_A v_A \ell_c x(h_A + \tfrac{1}{2} v_A^2)] = \frac{\dot{m}_p}{NL} (h_p + \tfrac{1}{2} V_w^2) dy$$

Integration gives

$$\rho_A v_A \ell_c x(h_A + \tfrac{1}{2} v_A^2) = \frac{\dot{m}_p}{NL}(h_p + \tfrac{1}{2} V_w^2)\, y$$

which, by the continuity equation, simplies to

$$C_{p_A} T_A + Q + h_B^{(o)} + \tfrac{1}{2} v_A^2 = C_{p_A} T_p + Q + h_B^{(o)} + \tfrac{1}{2} V_w^2$$

$$C_{p_A} T_A + \tfrac{1}{2} v_A^2 = C_{p_A} T_p + \tfrac{1}{2} V_w^2$$

Equations for control volume (B):

Continuity Equation in (B)

$$\rho_B v_B \ell_c (x_n - x) = \frac{d\dot{m}_n}{N} + (\rho_B + d\rho_B)(v_B + dv_B)\ell_c(x_n - x - dx)$$

$$d[\rho_B v_B \ell_c (x_n - x)] = -\frac{d\dot{m}_n}{N}$$

y-Component of the Momentum Equation in (B)

$$-\rho_B v_B^2 \ell_c (x_n - x) + \frac{d\dot{m}_n}{N} v_B + (\rho_B + d\rho_B)(v_B + dv_B)^2 \ell_c (x_n - x - dx)$$

$$= P\ell_c(x_n - x) - (P + dP)\ell_c(x_n - x - dx) - P\ell_c\, dx$$

$$d[\rho_B v_B^2 \ell_c (x_n - x)] + \ell_c (x_n - x) dP = -\frac{d\dot{m}_n}{N} v_B$$

Combination with the continuity equation gives,

$$\rho_B v_B dv_B + dP = 0$$

Energy Equation in (B)

$$\rho_B v_B \ell_c (x_n - x)[h_B + \tfrac{1}{2} v_B^2] = \frac{d\dot{m}_n}{N}[h_B + \tfrac{1}{2} v_B^2]$$

$$+ (\rho_B + d\rho_B)(v_B + dv_B)\ell_c(x_n - x - dx)[h_B + dh_B + \tfrac{1}{2}(v_B + dv_B)^2]$$

$$d[\rho_B v_B \ell_c (x_n - x)(h_B + \tfrac{1}{2} v_B^2)] = -\frac{\dot{m}_n}{N}(h_B + \tfrac{1}{2} v_B^2)$$

Substituting in the continuity equation yields

$$d\left(h_B + \tfrac{1}{2} v_B^2\right) = 0$$

which may be integrated to give

$$C_{p_B} T_B + h_B^{(o)} + \tfrac{1}{2} v_B^2 = + \tfrac{1}{2} v_{B_o}^2 + C_{p_B} T_{B_o} + h_B^{(o)}$$

$$C_{p_B} T_B + \tfrac{1}{2} v_B^2 = C_{p_B} T_{B_o} + \tfrac{1}{2} v_{B_o}^2$$

Therefore, the pertinent equations for the case of no mixing are

$$\rho_A v_A \ell_c x = \frac{\dot{m}_p}{NL} y$$

$$\frac{\dot{m}_p}{NL} y \, dv_A + \ell_c x dP = \frac{m_p}{NL}(V_w - v_A) dy$$

$$C_{p_A} T_A + \tfrac{1}{2} v_A^2 = C_{p_A} T_p + \tfrac{1}{2} V_w^2$$

$$d[\rho_B v_B \ell_c (x_n - x)] = -\rho_B a_B \left(\frac{2}{\gamma_B + 1}\right)^{\frac{\gamma_B + 1}{2(\gamma_B - 1)}} \ell_t \, dy$$

$$\rho_B v_B dv_B + dP = 0$$

$$C_{p_B} T_B + \tfrac{1}{2} v_B^2 = C_{p_B} T_{B_o} + \tfrac{1}{2} v_{B_o}^2$$

$$P = \rho_A \frac{R_o}{m_A} T_A = \rho_B \frac{R_o}{m_B} T_B$$

$$C_{p_A} T_A = \frac{a_A^2}{\gamma_A - 1}, \qquad C_{p_B} T_B = \frac{a_B^2}{\gamma_B - 1}$$

$$a_A^2 = \frac{\gamma_A P}{\rho_A}, \qquad a_B^2 = \frac{\gamma_B P}{\rho_B}$$

In non-dimensional form the equations become

$$\bar{\rho}_A \bar{v}_A \xi = G\eta$$

$$G\eta d\bar{v}_A + \frac{\xi}{\gamma_B M_o^2} d\bar{P} = G(\bar{V}_w - \bar{v}_A)d\eta$$

$$\bar{C}_{p_A}\bar{T}_A + \frac{\gamma_B - 1}{2} M_o^2 \bar{v}_A^2 = \bar{C}_{p_A}\bar{T}_P + \frac{\gamma_B - 1}{2} M_o^2 \bar{V}_w^2$$

$$d[\bar{\rho}_B \bar{v}_B(1 - \xi)] = -\frac{B\bar{P}}{M_o \bar{a}_B} d\eta$$

$$\bar{\rho}_B \bar{v}_B d\bar{v}_B + \frac{1}{\gamma_B M_o^2} d\bar{P} = 0$$

$$\bar{T}_B + \frac{\gamma_B - 1}{2} M_o^2 \bar{v}_B^2 = 1 + \frac{\gamma_B - 1}{2} M_o^2$$

$$\bar{P} = \bar{\rho}_A \bar{T}_A \frac{\bar{m}_B}{\bar{m}_A} = \bar{\rho}_B \bar{T}_B$$

$$\bar{C}_{p_A}\bar{T}_A = \frac{\gamma_B - 1}{\gamma_A - 1} \bar{a}_A^2, \qquad \bar{T}_B = \bar{a}_B^2$$

$$\bar{a}_A^2 = \frac{\gamma_A}{\gamma_B} \frac{\bar{P}}{\bar{\rho}_A}, \qquad \bar{a}_B^2 = \frac{\bar{P}}{\bar{\rho}_B}$$

The momentum equation for control volume (B) can be integrated by finding a relation for $\bar{\rho}_B$ in terms of $\bar{v}_B$ and $\bar{P}$.

$$\bar{\rho}_B = \frac{\bar{P}}{\bar{a}_B^2}$$

$$\bar{a}_B^2 = 1 - \frac{\gamma_B - 1}{2} M_o^2 (\bar{v}_B^2 - 1)$$

Hence, the momentum equation becomes

$$- \frac{1}{(\gamma_B - 1)M_o^2} \left[\frac{2\bar{v}_B d\bar{v}_B}{\bar{v}_B^2 - 1 - \frac{2}{(\gamma_B - 1)M_o^2}} \right] + \frac{1}{\gamma_B M_o^2} \left[\frac{d\bar{P}}{\bar{P}} \right] = 0$$

Giving upon integration

$$\bar{v}_B = \sqrt{1 + \frac{2}{(\gamma_B - 1)M_o^2} \left(1 - \bar{P}^{\frac{\gamma_B - 1}{\gamma_B}} \right)}$$

which leads to the relations

$$\bar{a}_B = \bar{P}^{\frac{\gamma_B - 1}{2\gamma_B}}$$

$$\bar{\rho}_B = \bar{P}^{1/\gamma_B}$$

We have two remaining differential equations:

$$G\eta d\bar{v}_A + \frac{\xi}{\gamma_B M_o^2} d\bar{P} = G(\bar{v}_w - \bar{v}_A)d\eta$$

$$d[\bar{\rho}_B \bar{v}_B (1 - \xi)] = - \frac{B}{M_o} \frac{\bar{P}}{\bar{a}_B} d\eta$$

which can be written to include just two dependent variables.

Boundary conditions:

at $\eta = 0$,

$$\bar{P}_o = \bar{v}_{B_o} = \bar{a}_{B_o} = 1 , \quad \xi_o = 0$$

$$\bar{v}_{A_o} = \bar{v}_w , \quad \bar{a}_{A_o} = \sqrt{\frac{\gamma_A - 1}{\gamma_B - 1} \bar{C}_{pA} \bar{T}_p}$$

At $\eta = 1$,

$$\bar{v}_{A_1} = b + \sqrt{b^2 + c}$$

$$\bar{P}_1 = 1 - \gamma_B M_o^2 (\bar{v}_{A_1} - 1)$$

$$\bar{a}_{A_1} = \sqrt{\frac{\gamma_A}{\gamma_B} [1 - \gamma_B M_o^2 (\bar{v}_{A_1} - 1)] \bar{v}_{A_1}}$$

where in this case

$$b = \frac{\gamma_A}{\gamma_B} \left[\frac{1 + \gamma_B M_o^2}{(\gamma_A + 1) M_o^2} \right]$$

$$c = \frac{2}{\gamma_B - 1} \left(\frac{\gamma_A - 1}{\gamma_A + 1} \right) \frac{1}{M_o^2} \left[\bar{Q} - \frac{\gamma_B - 1}{2} M_o^2 - 1 \right]$$

Also,

$$\bar{v}_{B_1} = \sqrt{1 + \frac{2\gamma_B}{\gamma_B - 1} (\bar{v}_{A_1} - 1)}$$

$$\bar{a}_{B_1} = \bar{P}_1^{\frac{\gamma_B - 1}{2\gamma_B}}$$

It is implied in the no-mixing flow model that at $\eta = 1$, $\xi = 1$. For this condition to hold the continuity equation for control volume (A) and the first jump condition give $G = 1$.

7. Conclusions

The assumptions, conditions, and resulting equations for an analytical model of the rotating detonation wave engine have been presented. The validity of this model rests upon the premise that the fluid flow is quasi-one dimensional when viewed in the system of the rotating detonation waves. The effects of turbulent mixing of the burned and unburned propellants are to be estimated by applying the alternative limiting conditions of complete mixing and no mixing. In both cases the resulting equations are a system of a first order ordinary differential equations with initial values related to the hydrodynamic jump conditions across the detonation waves.

Future work will consist of obtaining solutions to the equations, either exact or approximate, correlating the theory with data from the 100-lb engine tests, and using these results to aid the 1000-lb engine design effort.

II. EXPERIMENTAL STUDIES

A. THE GASEOUS, 100-LB THRUST MOTOR

The revision of the existing 100-lb thrust motor began with modifications which make it possible to change the injector faces, throat sections, and the axial length of the combustion chamber quite rapidly. These modifications will make it possible to study the effect of L*, the characteristic length, on the performance of the 100-lb thrust motor. Also, the interchangeability of the injector face on the modified 100-lb thrust motor will enable the effect of mixture ratio and injector pressure to be determined.

Originally the motor was located in a pit 11 feet deep in the center of the isolation cell. However, since the initiation of the contract, the motor has been moved to ground level. The relocation of the motor will facilitate day by day modifications and checks that must be carried out, also, the new location should make it possible to obtain photographs of the exhaust jet more easily.

The propellant feed system has also been modified by the installation of a new Hoke pressure regulator which appears to have a zero drift characteristic. The original pressure regulator was being operated above its maximum pressure limit which resulted in an extensive drift in the injector pressure between runs.

The fire controller has also been extensively modified. With the instrumentation in its original configuration there appeared to be an interconnection between the fire controller or time-delay spark unit and the oscilloscope trigger circuit. The revision of the fire controller and the relocation of both the oscilloscope and the time delay spark unit have apparently eliminated this interconnection.

The original instrumentation has been reassembled and relocated. This entire system, solenoid valves, injector pressure transducers and associated instrumentation, oscillograph, fire controller, time-delay spark unit, etc., has been checked by sequencing the motor with gaseous nitrogen, see Fig. 4, a schematic diagram of the revised test setup. Also see Figs. 5 and 6 for photographic details of the test setup. One of the oscillograph records for this shakedown phase is shown in Fig. 7. The record shows the essential mechanical operations plus the injector pressure and the ignition of the motor.

The Kistler pressure transducer instrumentation used to record the chamber pressure as a function of time, was installed in the 100-lb thrust motor and a live run made. Since these pressure traces were completely unsatisfactory, the chamber pressure instrumentation has been removed from the motor and installed

in a detonation tube. It is believed that this will facilitate the detection of the source of a high frequency oscillation, that has been superimposed on the pressure trace, more efficiently than could be done in the 100-lb thrust motor. This configuration will also make it possible to obtain dynamic pressure calibrations of the transducer by comparing the experimental results in the tube with the theoretical results predicted from non-steady, one-dimensional flow theory. An example of such a pressure trace utilizing the Kistler pressure transducer with the voltage displayed on the Tektronix Model 555 oscilloscope is shown in Fig. 8. The horizontal sweep time is 50 μ-sec/cm (cm = large division). While it is apparent that some high-frequency oscillations in the trace occur that are most pronounced immediately after the passage of the first wave, the vertical deflection (pressure) decreases to about one-third its value immediately behind the wave in about 400 μ-sec. This is in good agreement with theory. The second pressure pulse (at about 460 μ-sec) is a reflected shock wave from the diaphragm located at the end of the tube.

The thermocouples used to measure the wall temperature of the combustion chamber will probably be checked and dynamically calibrated in much the same way as the Kistler pressure transducer.

During the period in which the pressure transducer is being evaluated and calibrated, two high-speed framing cameras and one time exposure camera are being installed in the isolation cell. These high-speed framing cameras, a 16 mm Fastax and a 16 mm Beckman and Whitley, will obtain photographs of the exhaust. The velocity of the detonation wave and also any acceleration, whether a positive or negative, can be determined from these photographs. The photographs from the time exposure camera will ascertain the shape of the jet and help shed some light on the velocity pattern of the exhaust jet.

These cameras have been installed in the test cell, and the electronic unit necessary to sequence them is nearing completion.

Special Instrumentation

(a) Chamber Pressure.—The chamber pressure instrumentation consists of a Kistler Model 603 quartz crystal pressure transducer, the output of which is fed into a Kistler Model 566M charge amplifier. The output of the amplifier is applied to the CRT of a Tektronix Model 555, dual-beam oscilloscope and photographed with a Polaroid oscilloscope camera. The entire system should have a rise time < 2 μ-sec.

(b) Combustion Chamber Wall Temperature.—The wall temperature of the combustion chamber will probably be measured with a Nanmac film thermocouple (10 μ-sec rise time) in conjunction with a voltage amplifier and the Tektronix Model 555 oscilloscope. The fast rise of this type of thermocouple will make it possible to predict steady state heat transfer rates with a high degree of accuracy.

(c) Exhaust Jet.—The Fastax 16 mm framing camera is rated at approximately 7000 frames per second which will give about one frame per revolution of the detonation wave. This camera also has sufficient film capacity (100 ft) to record the entire run for run times of less than one second.

The Beckman and Whitley high-speed framing camera has a framing rate of about 26,000 frames per second but due to its limited film capacity (33-7/8 in.), only approximately 8 milliseconds of the run can be observed. Even though only a short portion of the run can be recorded, the high framing rate will yield much more accurate data on wave velocities and accelerations than is possible with the Fastax camera.

The photographs from the time-exposure camera will show the shape of the jet which in turn should provide some information concerning the nature of the expansion processes of the exhaust gases.

B. TEMPERATURE AND PRESSURE EFFECTS ON HYDROGEN-OXYGEN DETONATION VELOCITIES

The experimental setup has been completed. The additional items of equipment inlcude the following:

1. A stainless steel, vacuum-jacketed vessel to contain the coiled detonation tube and the low temperature liquid (see Fig. 9).

2. An exhaust fan to eliminate noxious fumes and combustible gases from the isolation cell.

3. A CMC Model 727-BN time interval counter capable of recording time intervals to an accuracy of $\pm$ 0.1 μ-sec.

It was decided that three different cooling fluids would be utilized. The first, normal propyl alcohol, used by Moyle[15] in his experiments, would be utilized from room temperature down to near its freezing point, about 160°K. The second, isopentane would be utilized to cover the range in temperature from 160°K to about 102°K, where it freezes. The range from 102°K down to 90°K (the vapor saturation temperature of oxygen at one atmosphere) would be covered utilizing liquid nitrogen pressure-regulated at a particular pressure to obtain the temperature corresponding to that vapor pressure of nitrogen. It is to be noted that cold nitrogen vapor initially at about 80°K is bubbled through the bath to cool either of the two fluids, normal propyl alcohol or isopentane in the higher temperature range. Table VI shows the temperature and pressure regions to be covered in the experiments and the cooling fluid to be used in the various temperature regions.

The stainless-steel coiled detonation tube utilized in the experiments has an I.D. of 0.25 in. similar to the one used by Moyle. It is approximately 25 ft long with the middle 12 ft submerged in the bath and used for the vel-

ocity measurement. Three ionization probes are installed 6 feet apart allowing the detonation velocity to be measured over two 6-foot intervals in the same run, affording a check that the wave has reached its steady-state Chapman-Jouguet velocity.

Preliminary tests were made in the coiled tube to check the fact already noted by Moyle, i.e., that the detonation velocity measured in a 0.25 in. I.D. tube coiled to a ten-inch diameter is very close (about 0.5% less) than the detonation velocity measured in a straight tube. These were also run to establish that at room temperature, H_2-O_2 detonations propagated at a constant Chapman-Jouguet velocity over the 12-foot length of the coil situated inside the bath.

The first series of experiments were performed to check the results of Moyle at one atmosphere and at different mixture ratios of hydrogen and oxygen from room temperature down to 160°K. The experiments were performed in the same manner as Moyle: normal propyl alcohol was utilized as the cooling fluid with cold nitrogen vapor used to cool the alcohol to the desired temperature. After each run the coil was removed from the bath and allowed to warm up to room temperature to melt the combustion products (H_2O) that had frozen in the tube. The tube was dried under a vacuum and recharged with the H_2-O_2 mixture and then replaced in the bath. The results of these experiments are shown in Fig. 10. Although the same mixture ratios were not employed, it is believed that the experimental verifications of Moyle's data can now be established. It had been hoped that in order to make a large number of runs in a minimum of time, the coiled tube could remain in the cooling bath between runs and the frozen combustion products eliminated by one of the following methods:

1. Purge coiled tube with dry N_2 immediately after run.
2. Sublime the ice by means of a vacuum.
3. Utilize a helium shock-tube driver section upstream of the coil and initiate the detonation wave with shock wave with the resulting helium piston gases purging the tube of H_2O.

The first two methods appeared to have no success. Elimination of the ice was deemed successful if a series of runs made at one low temperature yielded the same detonation velocity. Since the velocity was observed to change by about 5% it was concluded that ice was still accumulating on the inside walls of the tube. The third method, employing the helium shock tube driver appeared to be successful inasmuch as the detonation velocities were the same for several runs at moderate sub-freezing temperatures and the results agreed with the control experiments performed by removing the tube from the bath for each run. However, at lower temperatures it appeared as though the H_2O was not being removed rapidly enough by the He piston gases and ice was beginning to form.

The following decision has been made: the tedious method of removing the

coil from the bath will be utilized and the pressure and temperature region shown in Table VI will be investigated down to the freezing point of isopentane (112°K). Since the bath will be at one atmosphere for these runs, the cover will not have to be unbolted and rebolted after every run, a time consuming feature if LN_2 is employed as the coolant. By utilizing this technique, it will not be possible to check the region from 90°K to 112°K. However only a very small amount of the data was to be recorded in this range anyway (as is evident by examining Table VI), due to the higher saturation temperatures of oxygen at increased pressure.

C. DETONATION THROUGH HETEROGENEOUS, LIQUID-GAS MEDIA

A system involving a condensation chamber has been fabricated and instrumented and will be used to appraise the characteristics and limitations of the condensation system for droplet formation. This system will utilize condensation of one component of a mixture due to the temperature decrease associated with an isentropic expansion of the gases in the chamber. At the same time it will provide a means for determining the capabilities of the schlieren system, which will be used on the detonation tube as well. Figure 11 shows a view of the condensation chamber with glass windows as well as one leg of the schlieren system involving 6 in. diameter optics.

The schlieren system is almost completed and is being tested at various degrees of magnification using supplemental lenses. It is believed that the well known limitation of film speed and resolution will limit the magnification to between five and ten times natural size utilizing for exposure the light that is available from the high-voltage (25 kilivolt) short duration (about 0.1 μ-sec) light source.

The detonation tube has been fabricated in its component pieces and is ready for final assembly. Tests on mixtures containing the very small droplets produced by the condensation technique will be performed first. The instrumentation involved for this phase will consist of the schlieren system utilizing spark photography, ionization probes to determine detonation wave velocity, and a thermocouple and pressure transducer to determine the state of the mixture prior to detonation.

An injection system capable of producing larger droplets of either fuel or oxidizer is under consideration.

D. GEOMETRICAL TESTS

The experimental setup described in the last report[1] has been completed. The following changes have been made:

1. Glow-plug ignition is utilized instead of spark ignition to eliminate the spark-discharge interference with the electronic equipment.

2. Plexiglas windows with inferior optical quality were utilized initially in the test section due to the difficulty of fabricating curved glass windows.

3. A conventional schlieren system, employing 8-inch diameter mirrors with a short duration (0.1 μ-sec) high voltage (25 kilovolt) capacitor-discharge light source was employed.

4. A thyratron-triggered time delay unit consisting of a variable R-C time delay circuit is utilized to trigger the light source at the proper time.

5. A CMC Model 757-BN time-interval counter is used to measure the wave velocity in the straight or curved tube.

Figure 12 shows a view of experimental apparatus and Fig. 13 shows a detailed photograph of the curved-tube section.

Preliminary experiments have been performed utilizing the curved test section. The internal dimensions of the rectangular channel are 0.5 in. in the radial direction and 0.375 in. wide. The curved section has a 7.5 in. diameter, similar to the 100-lb thrust motor.

The experimental procedure is as follows:

1. The desired mixture of H_2 and O_2 is prepared in the mixing sphere and allowed to stand for 24 hours to insure uniform composition.

2. The detonation velocity is measured in the straight tube to ascertain the exact mixture ratio (utilizing the extensive data by Moyle).

3. The straight tube with the curved section is charged with the desired mixture and ignited.

4. The wave triggers the time-delay unit which in turn triggers the light source taking a schlieren photograph of the wave in the curved section of the tube.

Figures 14a and 14b are spark-schlieren photographs taken of a H_2-O_2 detonation with a mixture ratio of 60% H_2 by volume. The photographs were obtained on Polaroid Land film and two different magnifications were employed. The wave in each case has passed through about 3/4 of the curved section. Several interesting phenomena can be observed on the photographs. The leading edge of

the wave front appears to be at a slight angle to the radial direction, possibly showing the effect of the greater distance the wave must travel at the outer radius. Also, a multiply-reflected wave is visible in the burned gases behind the initial wave front. This effect has been noted in earlier experiments performed at this laboratory, but in these cases the reflected wave in straight tubes were always noted during the starting transient of the detonation, i.e., shortly after the transition from deflagration to detonation. These disturbances always died out and were not apparent at all if a sufficient distance was allowed for the wave to travel after its transition to a detonation wave. Since the distance between the point where the wave is initiated in the straight section and where the photographs are taken in the curved section is more than adequate for this disturbance due to the initiation of the wave to dissipate, it is concluded that the observed disturbance in the curved section is caused by the effect of the curved channel on the detonation process. Whether this disturbance dissipates with distance or is continually being generated must be established. It is possible that this disturbance could have an effect on the detonation wave structure and propagation velocity, if it persists. Utilizing many photographs of different waves at varying distances along the curved tube will check this effect in addition to establishing the effect of curvature on wave velocity and detonation limits.

III. STUDY PLANS FOR THE NEXT QUARTER

The theoretical studies described in Sections I-A and I-B of this report will be terminated early in this period. However experimental results will be utilized later to check both theoretical models. The study of the theoretical model describing the gas-dynamics involved with the rotating detonation wave engine will be continued. Approximate solutions of the equations for the complete mixing case as well as for the case without mixing will be attempted at an early date. This will be done to aid in understanding the experimental data from the 100-lb thrust motor in addition to providing a starting point for more accurate, detailed numerical solutions that could be obtained at a later date utilizing a digital computer.

A complete parametric study of the effects of injector geometry, propellant mass flow and mixture ratio, and chamber axial length and nozzle throat size, on the measurable detonation properties, i.e., wave velocity, chamber pressure, and wall temperature will be made for the 100-lb thrust motor. These results will be checked with the theoretical results predicted by the study described in Section I-C of this report and in Reference 1.

The maximum possible range of pressure and temperature effects on H_2-O_2 detonation velocities will be studied.

Further experiments will be carried out on the effects of curvature and relief on detonation wave characteristics in the curved tube.

Experiments will be made to obtain phenomenalogical data on detonation waves passing through heterogeneous liquid-gas media.

Preliminary and then final design will begin on the 1000-lb thrust rotating detonation wave engine to be tested at the Willow Run rocket test site.

REFERENCES

1. Nicholls, A. J., and Cullen, R. E., et al., "The Feasibility of a Rotating Detonation Wave Rocket Motor," Univ. of Mich. Eng. Res. Inst. Report 05179-1-P, August 1962.

2. Cramer, F. B., "The Onset of Detonation in a Droplet Combustion Field," IX International Symposium on Combustion, 1962.

3. Webber, W. F., "Spray Combustion in the Presence of a Traveling Wave," IIIV International Symposium on Combustion, 1962.

4. Hanson, A. R., Donich, E. G., and Adams, H. S., "An Experimental Investigation of Impact and Shock Wave Breakup of Liquid Drops," Univ. of Minnesota, Inst. of Tech. Dept. of Aero. Eng. Res. Report 125, January 1956.

5. Lane, W. R., "Shatter of Drops in Streams of Air," Ind. Eng. Chem. 43, 1951.

6. Rabin, E., and Lawhead, R., "The Motion and Shattering of Burning and Nonburning Propellant Droplets," AFOSR TN-59-129, March 1959.

7. Engel, O. G., "Fragmentation of Waterdrops in the Zone Behind an Air Shock," J. of Res. NBS 60, 1958.

8. Hinze, J. O., "Critical Speeds and Sizes of Liquid Globules," App. Sci. Res., 1949.

9. Merrington, A. C., and Richardson, E. G., proc. Phys. Soc. (London) A 59, 1 (1947).

10. Williams, F. A., "Progress in Spray-Combustion Analysis," IIIV International Symposium on Combustion, 1962.

11. Hanson, A. R., and Domich, E. G., "The Effect of Liquid Viscosity on the Breakup of Droplets by Air Blast," Univ. of Minnesota, Inst. of Tech., Dept. of Aero. Eng. Res. Report 130, June 1956.

12. Gordon, G. D., "Mechanism and Speed of Breakup of Drops," J. of Applied Physics, Vol. 30, No. 11, November 1959.

13. Dodd, K. N., "On the Disintegration of Water Drops by Shock Waves," Royal Aircraft Establishment Tech. Note No. M.S. 64, May 1960.

14. Lane, W. R., and Green, H. L., "The Mechanics of Drops and Bubbles," G. I. Taylor Anniversary Volume, Cambridge Univ. Press (1956).

15. Moyle, M. P., "The Effect of Temperature on the Detonation Characteristics of Hydrogen-Oxygen Mixtures," Industry Program Report IP-195, The University of Michigan, Dec. 1956.

16. Morrison, R. B., "A Shock Tube Investigation of Detonation Combustion," Eng. Res. Inst. Report UMM-97, Univ. of Mich., January 1952.

17. Hayes, W. D., and Probstein, R. F., "Hypersonic Flow Theory," Academic Press, New York, 1959, Chapter VIII.

18. Penner, S. S., "Chemistry Problems in Jet Propulsion," Pergamon Press, New York, 1957.

19. Curran, A. N., et al., "Analysis of Effects of Rocket-Engine Design Parameters on Regenerative-Cooling Capabilities of Several Propellants," NASA TN D-66, Sept. 1959.

20. Sievers, G. K., et al., "Theoretical Performance of Hydrogen-Oxygen Rocket Thrust Chambers," NASA Tech. Rept. R-111, 1961.

TABLE I

THEORETICAL AND EXPERIMENTAL CORRELATION OF CRITICAL SIZE OF DROPLETS OF DIFFERENT FLUIDS FOR BAG-TYPE DROPLET BREAKUP

	Liquid	Surface Tension, dyne/cm S	Experimental Critical Velocity, ft/sec U	Experimental Critical Size, micron $(r)_{cr}$	Calculated Critical Size by Using Eq. (3) and Values of Experimental Critical Velocity, micron $(r)_{cr}$
Group (A)	Burning RP-1	11	92	100	75
	Burning RP-1	11	85	100	87.5
	Burning RP-1	11	82	100	98.5
	Non-Burning RP-1	38	95	100	240
	Non-Burning RP 1	38	125	100	140
Group (B)	Dow Corning 200-A Fluid	21.14	73.5	213	246
	Dow Corning 200-A Fluid	21.14	93.0	143	156
	Dow Corning 200-A Fluid	21.14	121.3	90	103
	Dow Corning 200-A Fluid	21.14	148.5	59	60.5
	Water	71.97	121.3	200	321
	Water	71.97	198.8	90	119
	Water	71.97	282.0	53	59.5
	Methyl Alcohol	22.2	74.4	235	263
	Methyl Alcohol	22.2	121	93	101
Group (C)	Water	72.75	84.3	300	665
	Water	72.75	109.5	205	377
	Water	72.75	157.3	135	180
	Water	72.75	238.5	60	73.5
	Methyl Alcohol	22.6	60	317	415
	Methyl Alcohol	22.6	84.3	165	208
	Methyl Alcohol	22.6	109.5	125	120
	Methol Alcohol	22.6	157.3	99	55

Experimental data for group (A) are taken from Ref. 6.
Experimental data for group (B) are taken from Ref. 11.
Experimental data for group (C) are taken from Ref. 4.

TABLE II

THEORETICAL AND EXPERIMENTAL CORRELATION OF CRITICAL SIZE OF BURNING AND NON-BURNING DROPLETS OF RP-1 FOR SHEAR-TYPE DROPLET BREAKUP

Liquid	Surface Tension, dyne/cm S	Experimental Critical Velocity, ft/sec U	Experimental Critical Size, micron $(r)_{cr}$	Calculated Critical Size by Using Eq. (5), micron $(r)_{cr}$
Burning RP-1	11	83	500	152
Burning RP-1	11	55	500	345
Non-Burning RP-1	38	93	500	411
Non-Burning RP-1	38	80	500	550

Experimental data are taken from Ref. 6.

TABLE III

THEORETICAL SHEAR-TYPE DROPLET BREAKUP TIMES FOR BURNING AND NON-BURNING DROPLETS OF RP-1 USING EXPERIMENTAL VALUES OF CRITICAL VELOCITY AND CRITICAL SIZE

Liquid	Surface Tension, dyne/cm S	Experimental Critical Velocity, ft/sec U	Experimental Critical Size, micron $(r)_{cr}$	Breakup Times Calculated by Using Eq. (4-a), sec
Burning RP-1	11	83	500	0.489×10^{-3}
Burning RP-1	11	55	500	1.16×10^{-3}
Non-Burning RP-1	38	93	500	0.925×10^{-3}
Non-Burning RP-1	38	80	500	1.29×10^{-3}

Experimental data are taken from Ref. 6.

TABLE IV

THEORETICAL SHEAR-TYPE DROPLET BREAKUP TIMES
OF LIQUID OXYGEN DROPLETS IN A STOICHIOMETRIC H_2-O_2 DETONATION

Radius of the Droplets, r(microns)	Reynold's Number, Re	Breakup Time Calculated by Using Eq. (4-a), t_b(sec)
500	30.8	0.89×10^{-7}
600	37	0.99×10^{-7}
700	43.1	1.0×10^{-7}
800	49.2	1.15×10^{-7}
900	55.6	1.22×10^{-7}
1000	61.6	1.25×10^{-7}

Surface tension of liquid oxygen = 13.2 dyne/cm (at T = 90°K)
Detonation velocity = 9400 ft/sec
Mole-fraction of hydrogen = 0.667
Viscosity of gas mixture = 0.894×10^{-3}]*
Density of gas mixture = 5.2×10^{-4} gm/cm^3]*
Density of liquid oxygen = 0.4299 gm/cm^3 (at T = 154.3°K)

*Corresponding to the condition behind the detached shock.

TABLE V

THE VARIATION OF DETONATION PARAMETERS AND HEAT
FLUX WITH MIXTURE RATIO

X_{H_2}	V_D, ft/sec	T_e, °R	q_w Dissociation Neglected, Btu/ft^2 sec	q_w Dissociation Included, Btu/ft^2 sec
0.40	6,879	5893	$1493\left(\frac{1}{x}\right)^{1/5}$	$1902\left(\frac{1}{x}\right)^{1/5}$
0.50	7,672	6314	1819	2589
0.60	8,620	6510	2135	3298
0.76	10,758	6484	2723	3776
0.80	11,262	6267	2683	3337

X_{H_2} = mole-fraction of H_2
V_D = detonation velocity
T_e = temperature behind the detonation
q_w = heat flux at the wall
x = distance behind detonation (ft)

TABLE VI

TEST CONDITIONS FOR THE PRESSURE AND TEMPERATURE EFFECTS ON H_2-O_2 DETONATION VELOCITIES

Mixture Ratios: 0.55, 0.67, 0.73, 0.80

Pressure, atm	Temperature, °K							
	Normal Propyl Alcohol			Isopentane or Liquid Nitrogen			Liquid Nitrogen	
1	300	200	146	125	110	112	95	90.2*
10	300	200	146	125				120*
30	300	200	146					140*
50	300	200	160					154*

*Boiling point of oxygen.

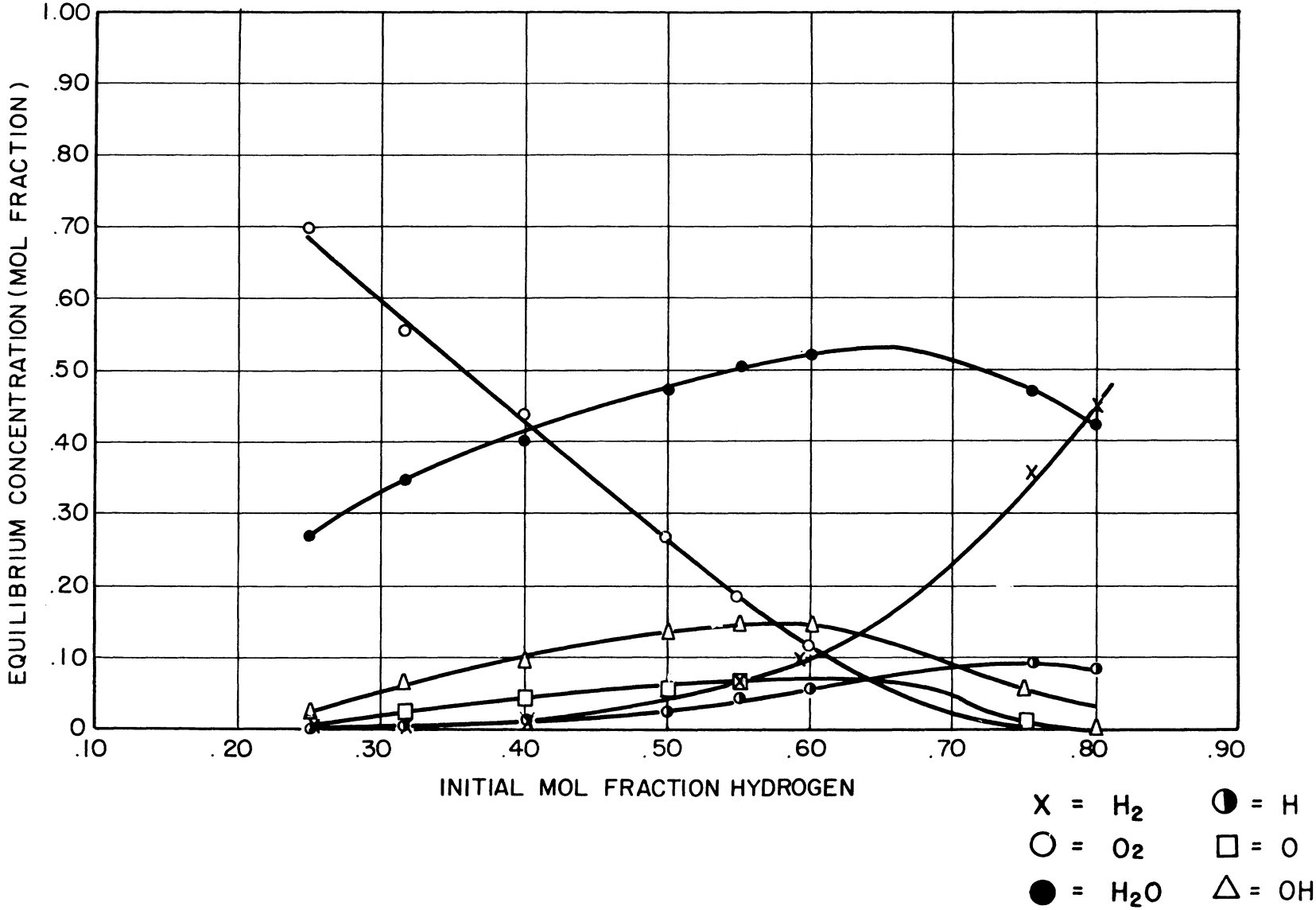

Fig. 1. Equilibrium concentration versus initial hydrogen content behind H_2-O_2 Chapman-Jouguet detonations. Initial temperature = 300°K; initial pressure = 1 atm.

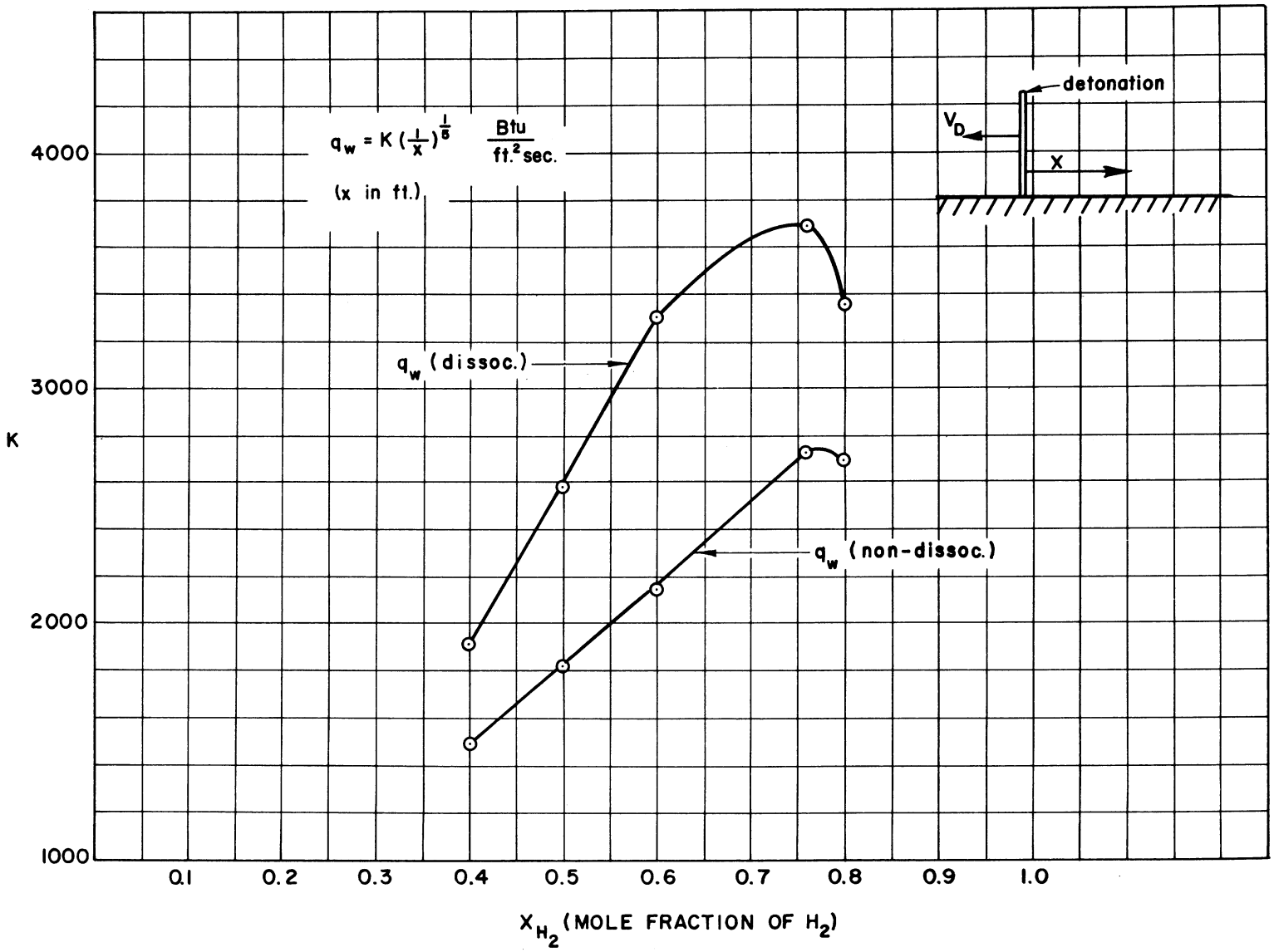

Fig. 2. Heat flux to the wall of the rotating detonation wave engine versus mixture ratio with and without dissociative recombination.

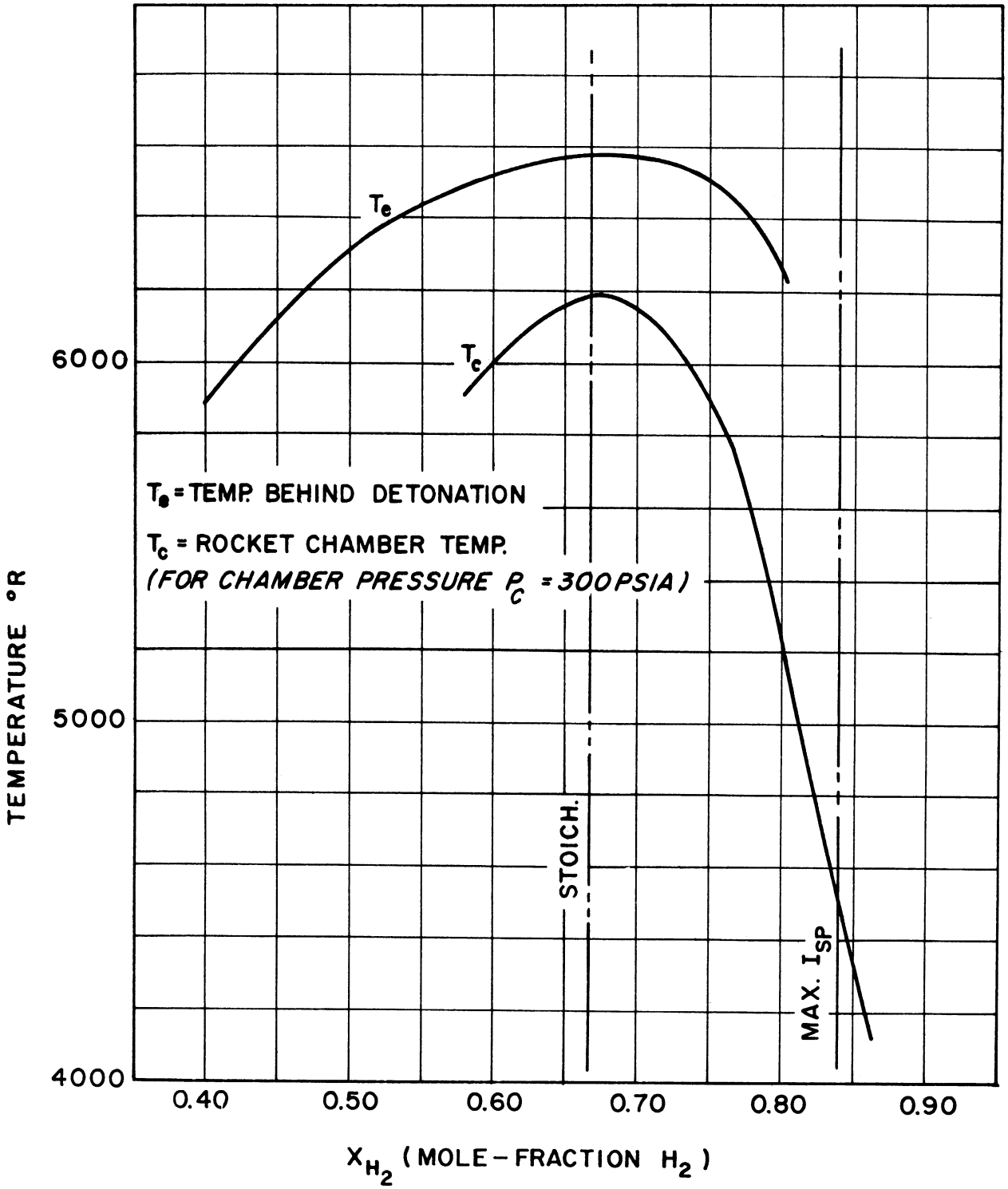

Fig. 3. H_2-O_2 Chapman-Jouguet detonation and combustion chamber temperatures as a function of mixture ratio.

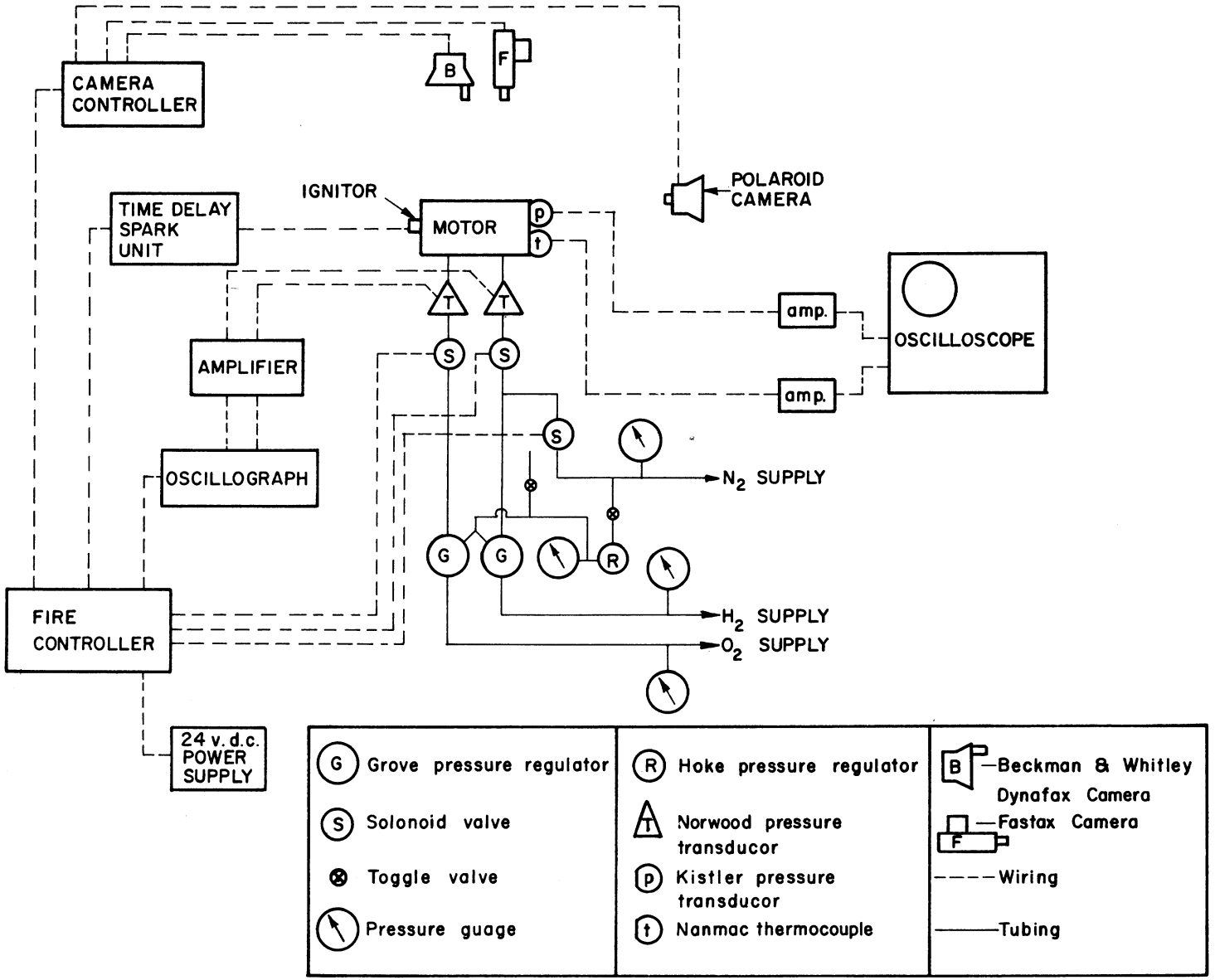

Fig. 4. Schematic diagram of test setup for 100-lb thrust motor.

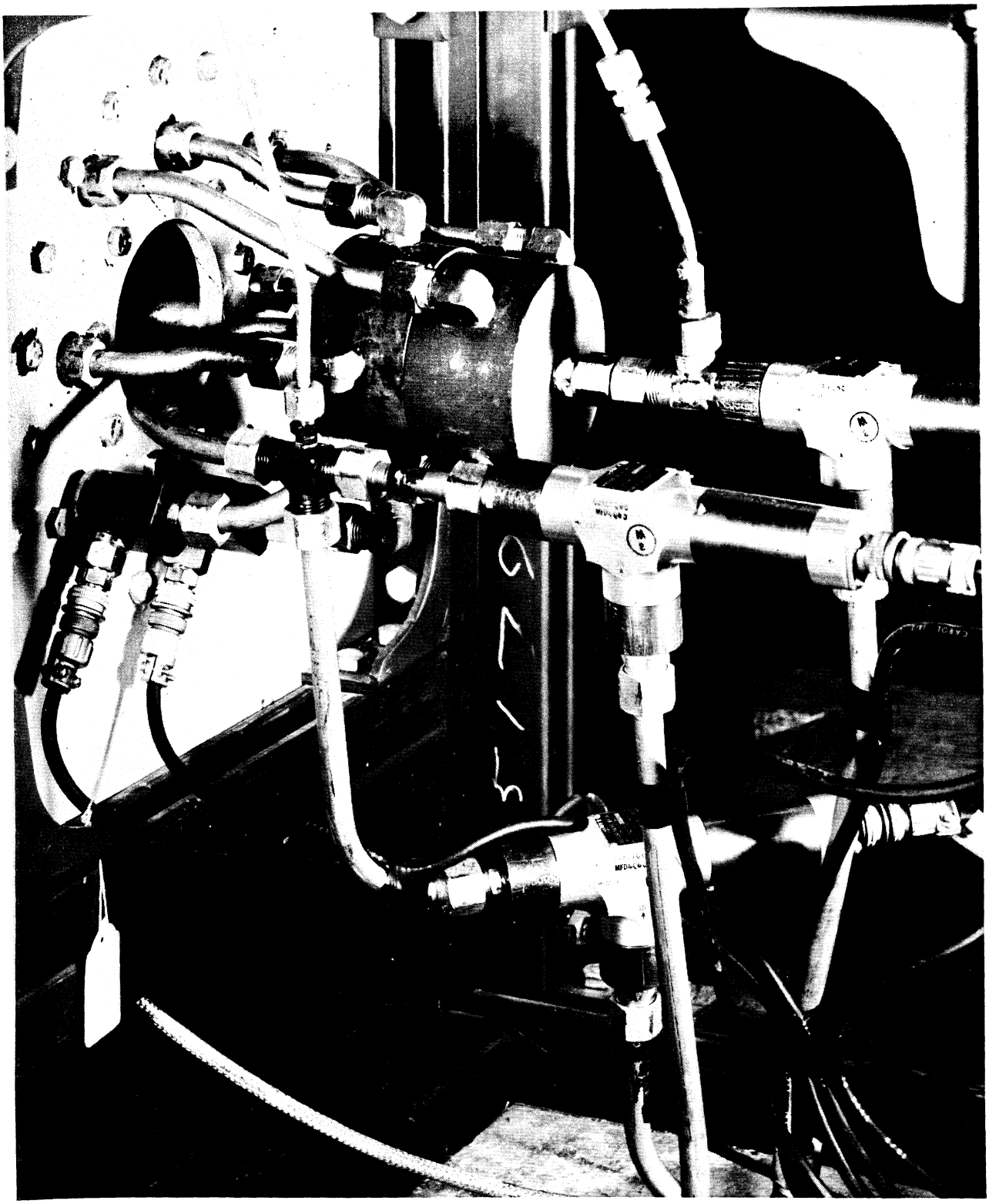

Fig. 5. Photograph of valve and injector manifold arrangement for 100-lb thrust motor.

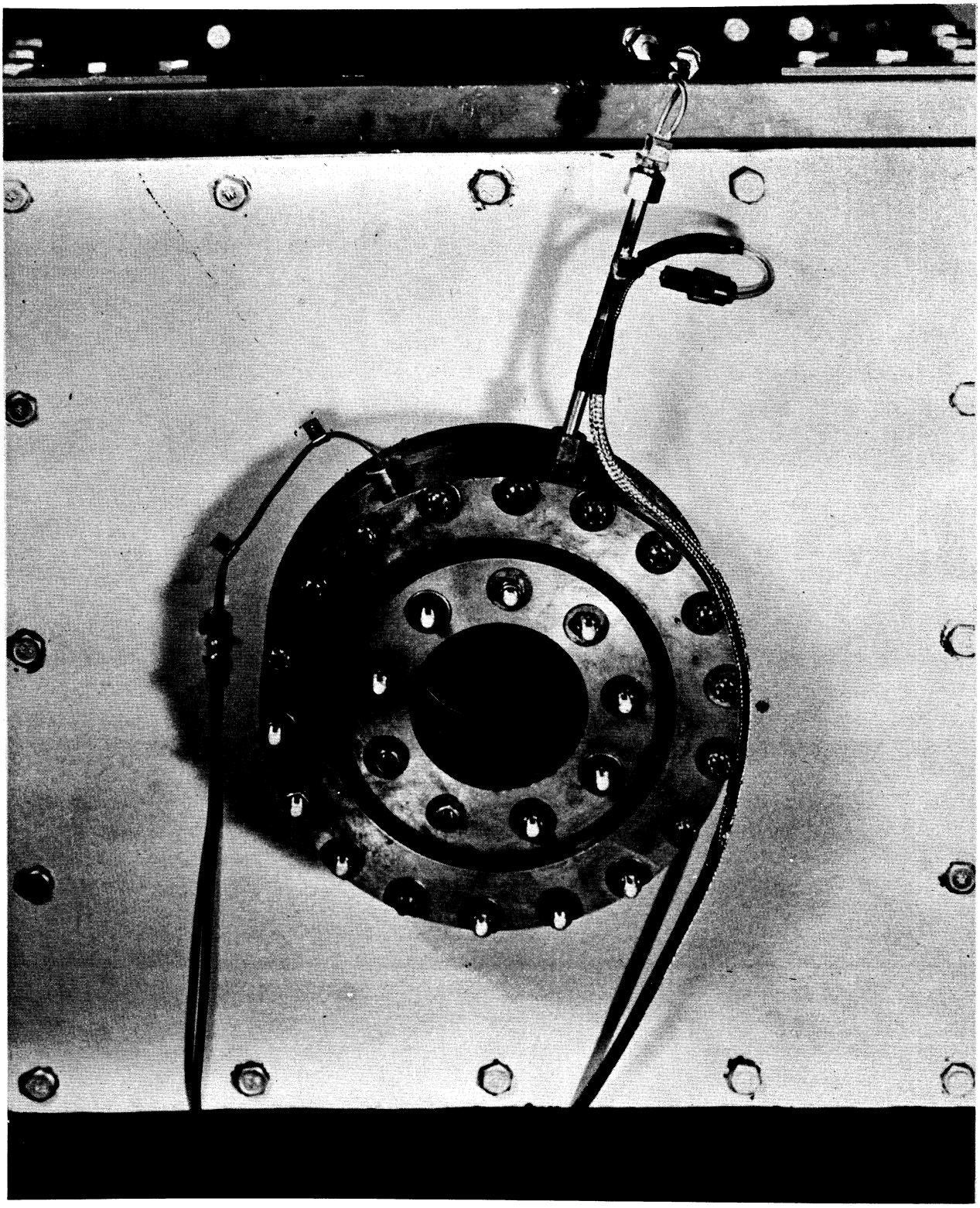

Fig. 6. Photograph of downstream end of 100-lb thrust motor.

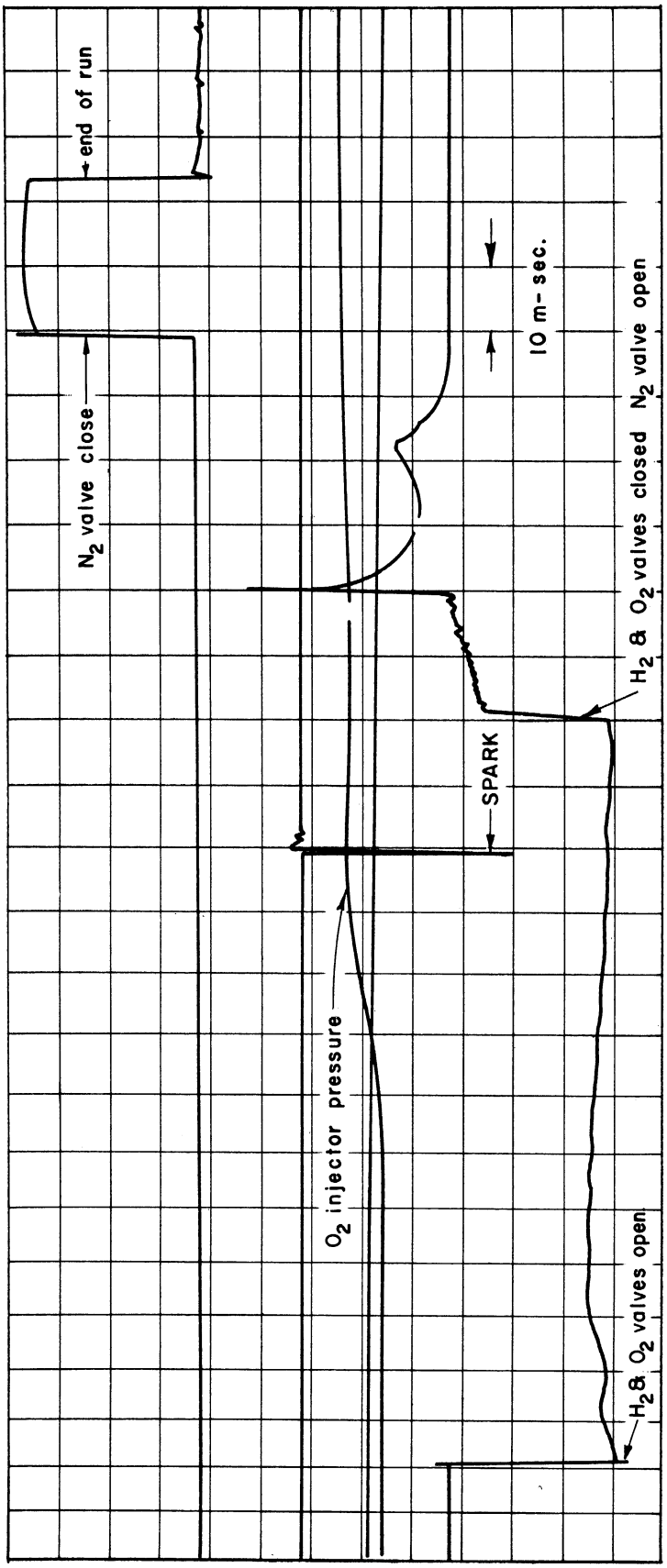

Fig. 7. Oscillograph record of essential mechanical operations, injector pressure, and ignition of 100-lb thrust motor.

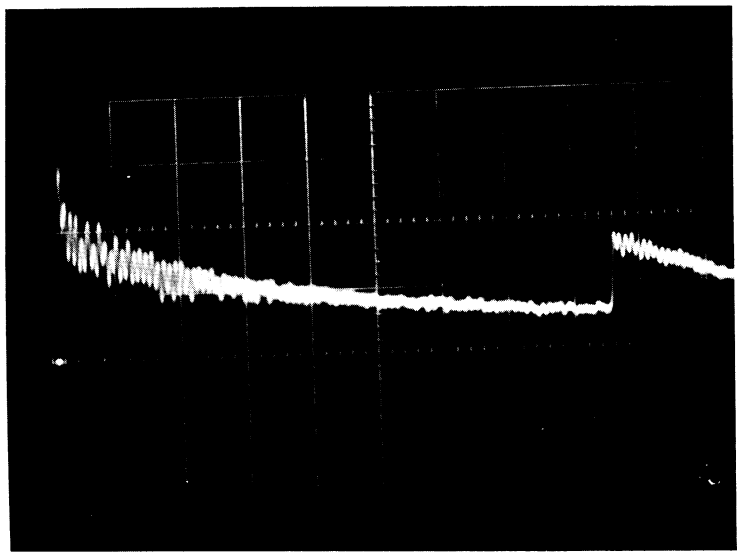

Fig. 8. Pressure trace of H_2-O_2 detonation wave in straight tube using the Kistler Model 603 pressure transducer.

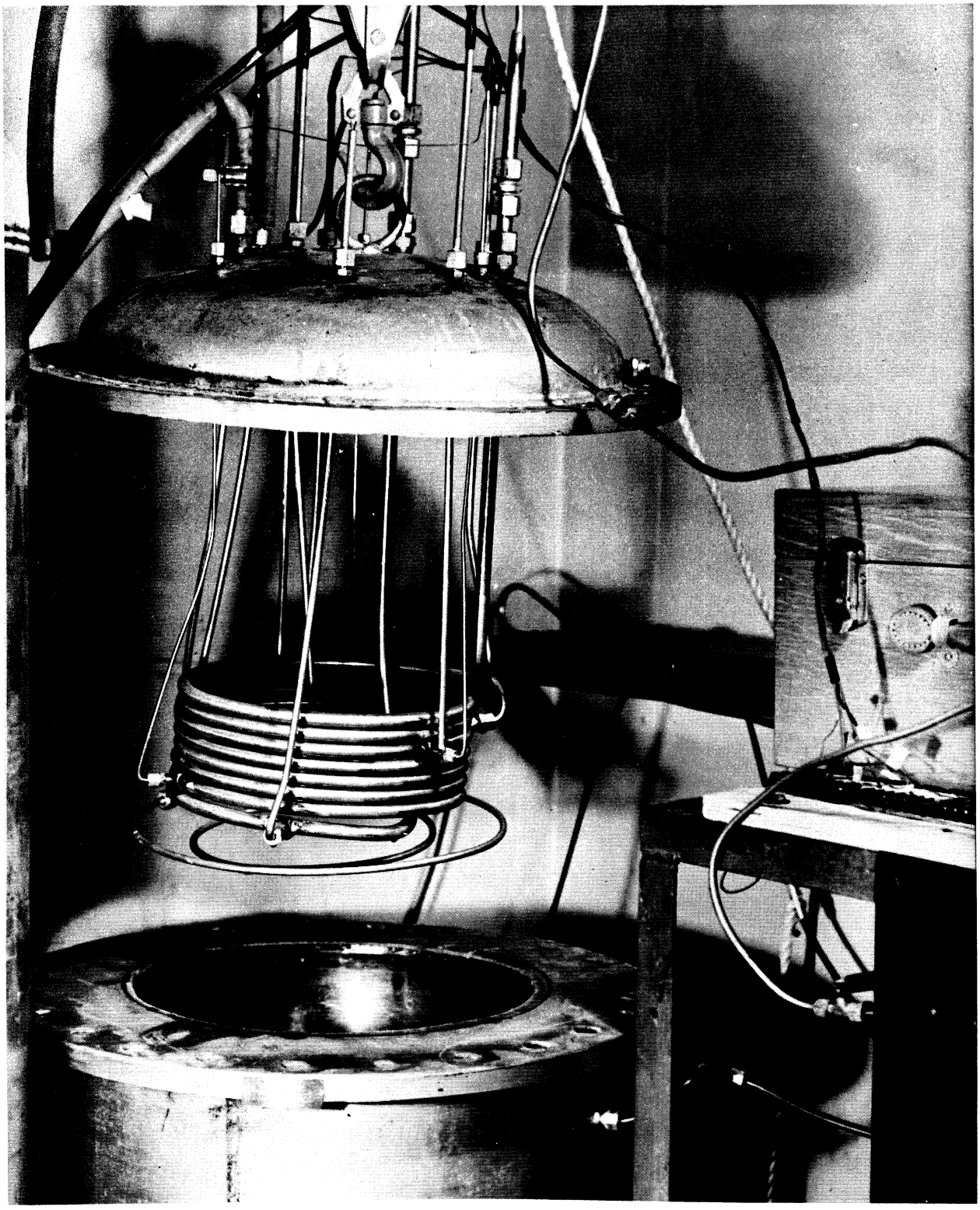

Fig. 9. Coiled tube and vacuum-jacketed vessel used in the pressure and temperature experiments.

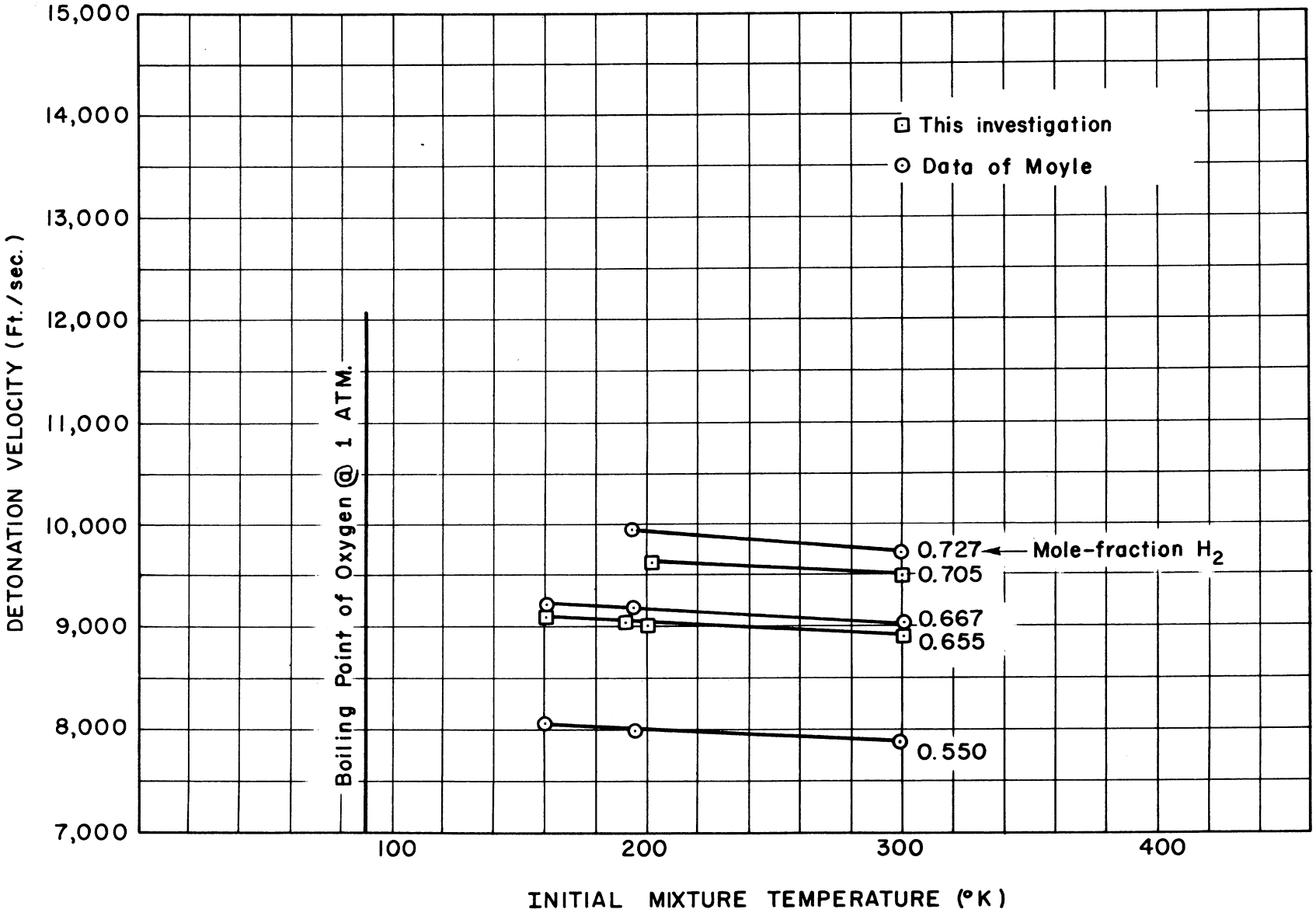

Fig. 10. Detonation velocity of H_2-O_2 gas at one atmosphere and at reduced temperatures.

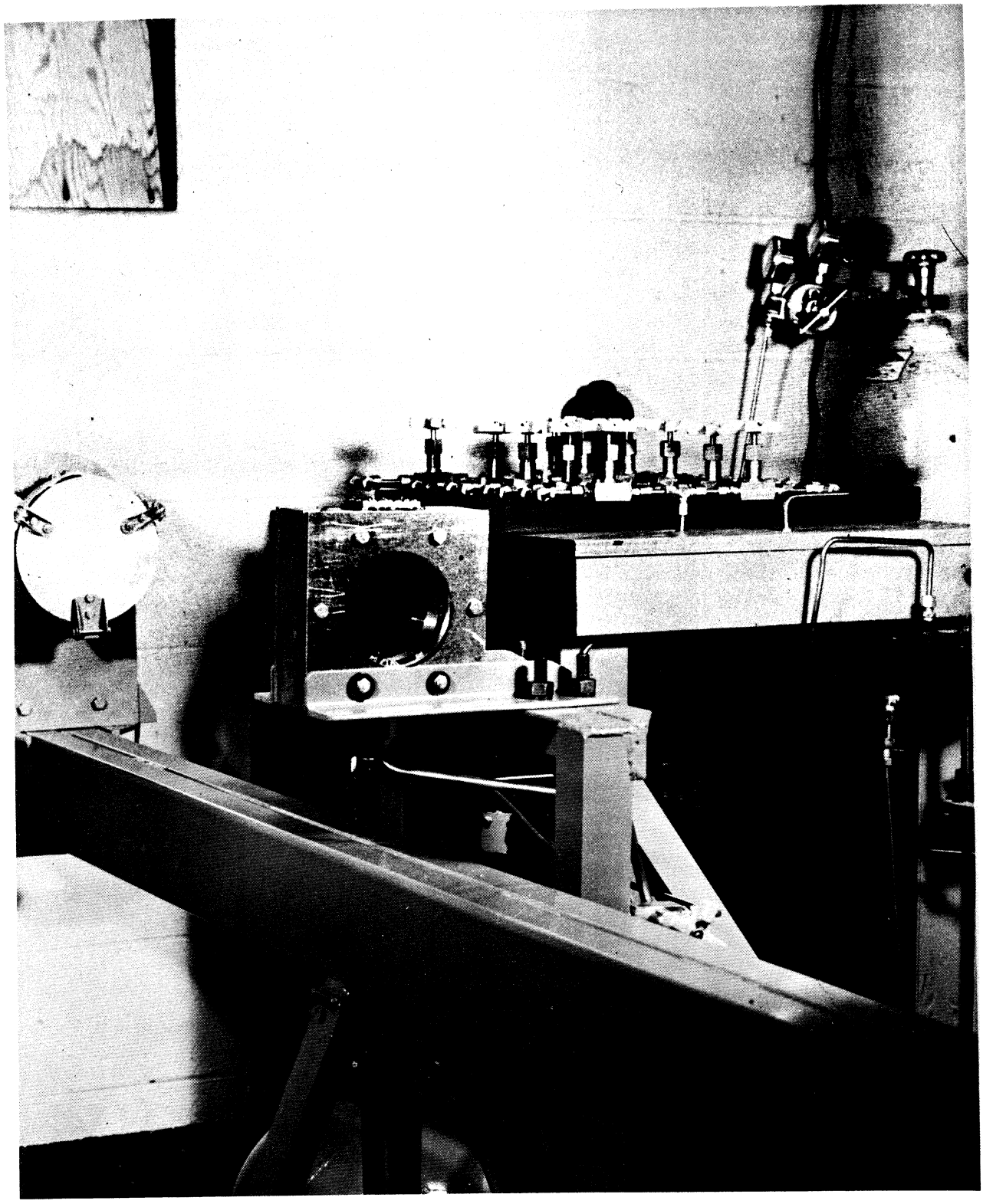

Fig. 11. Photograph of condensation chamber and schlieren system.

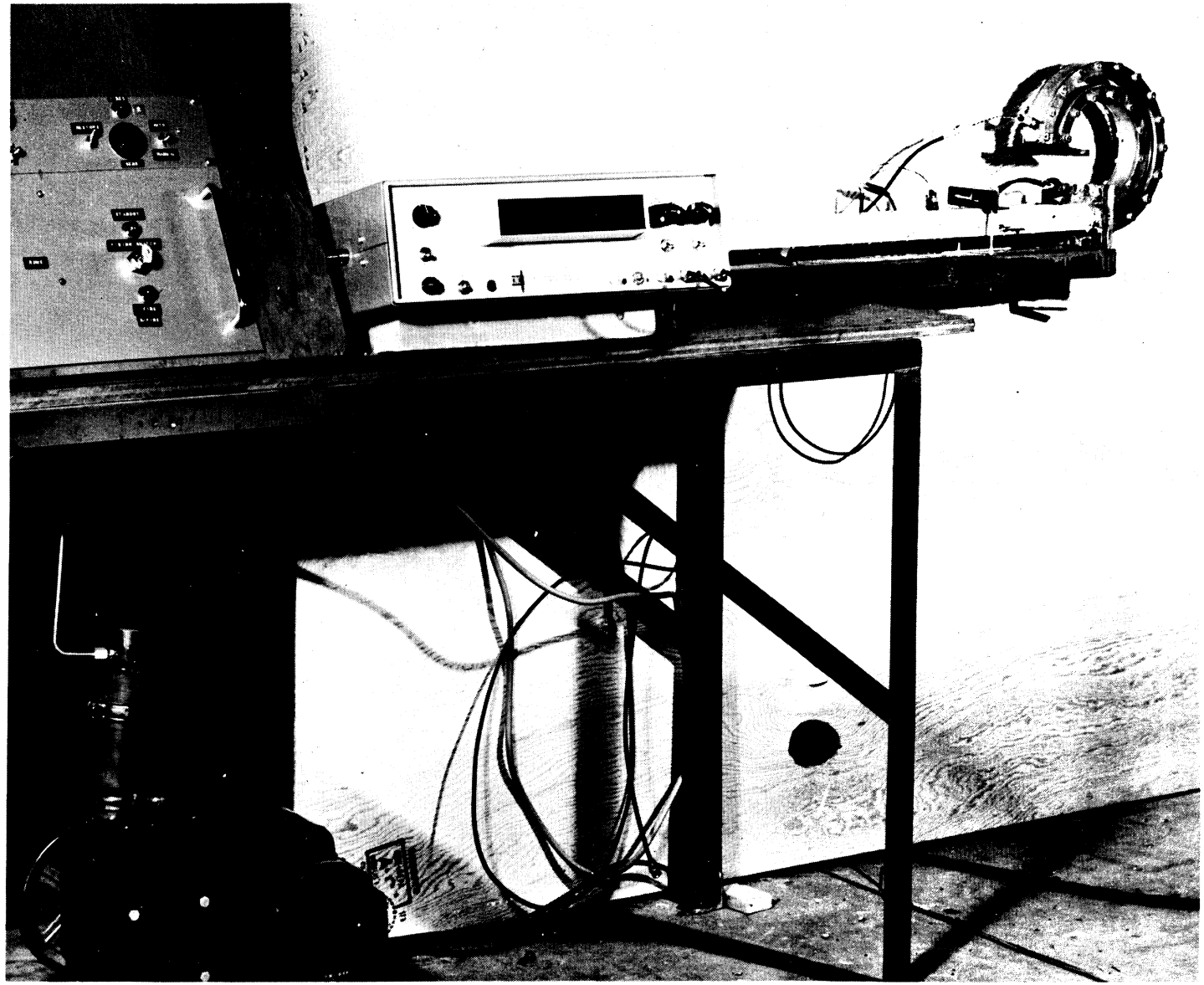

Fig. 12. Photograph of experimental equipment associated with the geometrical effect studies.

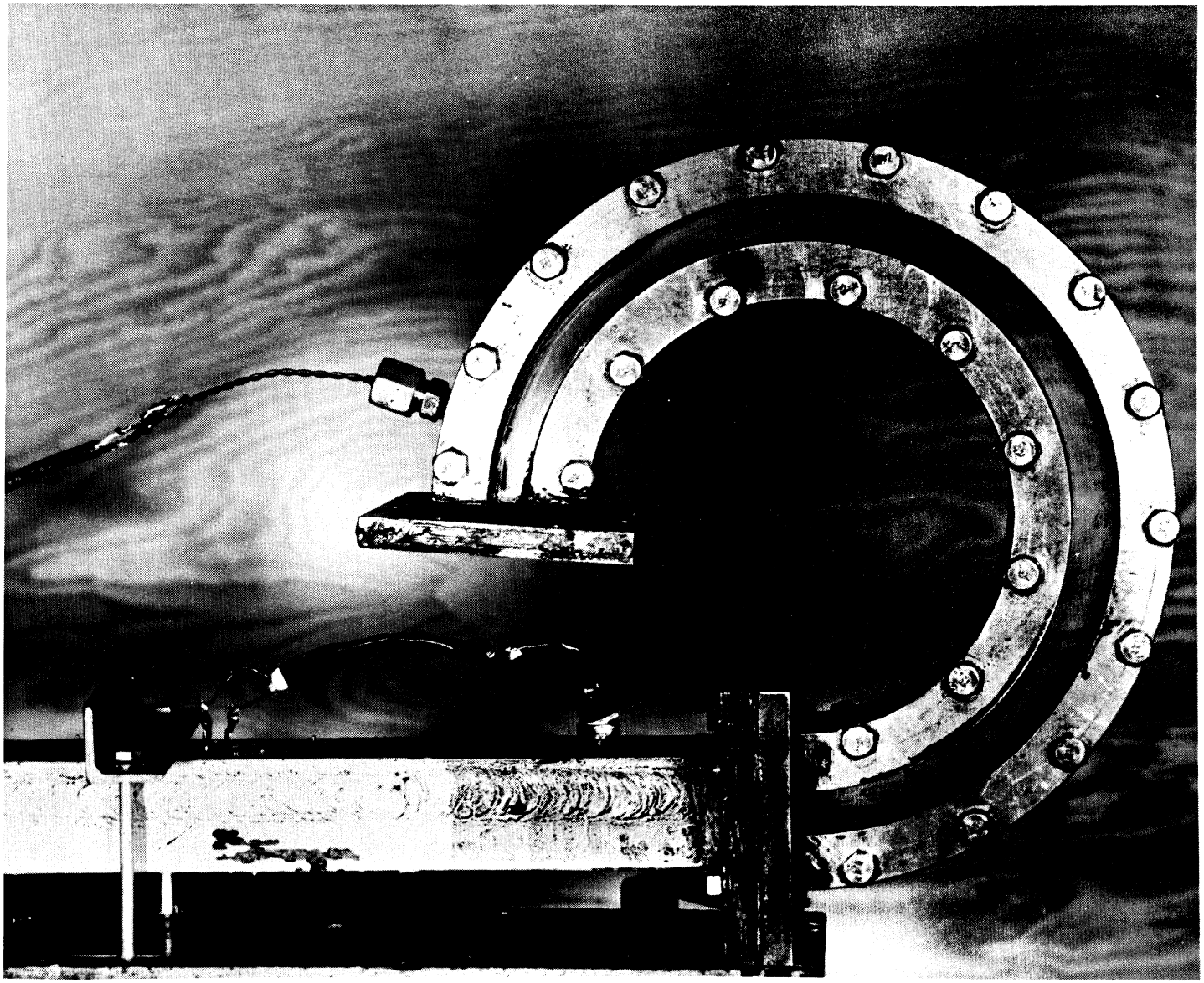

Fig. 13. Photograph of curved detonation tube section.

(a)

(b)

Fig. 14. Spark-schlieren photographs at different magnifications of two 60%, H_2-O_2 detonation waves passing through the curved test section.